Soil Biology and Biochemistry 178 (2023) 108959

Contents lists available at ScienceDirect

Soil Biology and Biochemistry

journal homepage: www.elsevier.com/locate/soilbio

Enhanced loss but limited mobility of pyrogenic and organic matter in continuous permafrost-affected forest soils

Marcus Schiedung [a,*], Severin-Luca Bellè [a], Carmen Hoeschen [b], Steffen A. Schweizer [b], Samuel Abiven [a,c,d]

[a] University of Zurich, Department of Geography, Winterthurerstrasse 190, 8057, Zurich, Switzerland
[b] Technical University of Munich, TUM School of Life Sciences, Department of Life Science Systems, Soil Science, Emil-Ramann-Str. 2, 85354, Freising, Germany
[c] École normale supérieure, Laboratoire de Géologie, Département de Géosciences, PSL University, Institut Pierre Simon Laplace, Rue Lhomond 24, 75005, Paris, France
[d] CEREEP-Ecotron Ile De France, ENS, CNRS, PSL University, Chemin de busseau 11, 77140, St-Pierre-lès-Nemours, France

ARTICLE INFO

Keywords:
Pyrogenic carbon
In-situ incubation
High-latitude soils
Soil carbon fractions
^{13}C-labeled organic matter
Nanoscale secondary ion mass spectrometry

ABSTRACT

Pyrogenic organic matter (PyOM) is a product of incomplete combustion during wildfires and an important pool of soil organic carbon (SOC). The dynamics of PyOM and SOC in boreal and permafrost-affected soils are largely unknown, while storing large amounts of global carbon and being vulnerable to climate change. Here, we traced the vertical mobility, allocation in soil fractions and decomposition losses of highly ^{13}C-labeled PyOM and its precursor ryegrass organic matter (grass OM) after two years of *in-situ* incubation in soil cores installed in the upper 10 cm of continuous (northern sites) and discontinuous to sporadic (southern sites) permafrost-affected forest soils in Northern Canada. At the northern sites, up to three times more PyOM was lost by decomposition (39% of initial) compared to the southern sites (11% of initial). Losses of grass OM were substantial (69–84% of initial) and larger in southern soils. The vertical incorporation was limited and >90% of recovered PyOM and grass OM were found at the applied depth (0–3 cm). The PyOM strongly interacted with mineral surfaces, as indicated by around 40% recovered in the mineral-associated heavy density fractions (<63 μm). Microscale analyses by SEM and NanoSIMS showed that PyOM was mainly allocated towards the fine fraction in a particulate and aggregated form, highlighting the importance of abiotic processes for the incorporation of PyOM in permafrost-affected soils. The grass OM was mainly recovered in the mineral fractions at southern soils with enhanced allocation towards mineral surfaces as well as increased distribution at the microscale after initial decomposition, while it remained as particulate OM in northern soils. Our results highlight that permafrost-affected boreal forest soils are sensitive to fresh PyOM and OM inputs with substantial losses. Especially PyOM persistence depended on site and soil specific properties and not solely on its physico-chemical persistence. The responses are decoupled for PyOM and non-pyrolyzed OM and require a better understanding to evaluate carbon feedbacks of high-latitude soils with global warming and associated shifts in vegetation and wildfire regimes.

1. Introduction

Soils of the high-latitudes in regions >60° north are estimated to store 30–40% of the total global soil organic carbon (SOC), which makes them a major contributor to the global carbon (C) cycle by covering only 15% of the land surface (McGuire et al., 2009; Hugelius et al., 2013; Köchy et al., 2015). High-latitude regions are predicted to experience major changes with global warming and surface temperature rises of up to 8 °C in the next decades (Hartley et al., 2012; Erdozain et al., 2019; IPCC, 2021), with an already reported warming of 2.3 °C between 1948 and 2016 for northern Canada (Zhang et al., 2019). The projected temperature rises specifically affect arctic and boreal soils where low temperatures and permafrost are major controlling factors of the SOC cycling (Schuur et al., 2015; Turetsky et al., 2020; Chen et al., 2021).

Wildfires are major disturbances of boreal forest ecosystems and annually 5–20 Mha (approx. 1%) of boreal forests are affected by wildfire with up to 7 Mha of forest and taiga located in Canada (Stocks et al., 2002; Flannigan et al., 2009). Pyrogenic organic matter (PyOM) is

* Corresponding author.
E-mail address: marcus.schiedung@geo.uzh.ch (M. Schiedung).

https://doi.org/10.1016/j.soilbio.2023.108959
Received 24 August 2022; Received in revised form 7 January 2023; Accepted 14 January 2023
Available online 18 January 2023

a product of incomplete combustion occurring during wildfires and can represent more than 15% of the initial vegetation biomass (Santín et al., 2016). Globally, PyOM production rates of 196–340 Tg C and losses of 89 Tg C by mineralization are estimated annually (Jones et al., 2019; Bowring et al., 2022). In soils, around 14% of the global SOC is predicted to be derived from pyrogenic sources, which makes PyOM an important component of the SOC pool (Reisser et al., 2016).

Thermal degradation and condensation reactions during pyrolysis turn PyOM into a continuum of highly condensed C-rich polyaromatic and aliphatic structures. This makes PyOM persistent to environmental degradation (biotic and abiotic), increases its residence time compared to non-pyrolyzed OM and changes its chemical and physical properties in terms of reactivity and mobility (Bird et al., 2015; Pingree and DeLuca, 2017). The PyOM continuum contains a significant proportion of fast cycling and easily available C fractions, which are found to be decomposed in the early stage after PyOM entered the soil (Spokas, 2010; Zimmerman, 2010; Singh et al., 2012b). The decomposability of PyOM depends on the fuel biomass, its composition as well as the production temperature, with higher persistence with increasing temperature due to increasing condensation and aromaticity (Preston and Schmidt, 2006; Singh et al., 2012a; Santos et al., 2021). It is reported that the proportion of PyOM to the bulk SOC increases with soil depth, indicating important vertical transport mechanisms and deep storage in soils (Soucémarianadin et al., 2015, 2019). While a few studies focused on the PyOM dynamic in soils under field conditions in temperate and tropical regions (e.g. Maestrini et al., 2014; Major et al., 2010; Singh et al., 2014), the fate of PyOM in permafrost-affected soils is largely unknown.

Temperature rises may enhance plant productivity of the high latitudes (Xu et al., 2013), which in turn could increase C inputs to soils. Simultaneously the frequency and intensity of wildfires will increase with high confidence (IPCC, 2021), which consequently may lead to a larger input of PyOM to soils. Laboratory-based experiments showed that high-latitude soils are sensitive to fresh OM, acting as energy and nitrogen (N) source (Wild et al., 2014, 2016). On ecosystem-scale, fresh OM input with warming induced vegetation changes may result in acceleration of SOC decomposition and a net loss (Hartley et al., 2012) or gain (Sistla et al., 2013) of total C. The fate of fresh OM and PyOM inputs, however, is largely unknown under field conditions and especially in permafrost-affected soils, which limits our understanding of C dynamics in the high-latitude regions vulnerable to climate change.

The cold climatic conditions in high-latitude regions cause a preservation of SOC and PyOM due to reduced microbial degradation and limited nutrient availability (Kaiser et al., 2007; Trumbore, 2009; Sistla et al., 2012; Schuur et al., 2015). Microbial activity is highest during summer months and when soils are partly unfrozen forming the active layer. Soils under continuous permafrost show generally higher SOC stocks and ages compared to soils under discontinuous or sporadic permafrost due to vertical mixing by cryoturbation induced by freezing and thawing, which incorporates OM deeper into the soil (Bockheim, 2007; Kaiser et al., 2007; Tarnocai and Bockheim, 2011; Schiedung et al., 2022). The mechanisms controlling the stabilization of SOC in permafrost soils are not clear so far and if PyOM follows the same mechanisms or is decoupled is unknown. A previous micro-scale study indicated that particulate organic matter in permafrost-affected soils creates hotspots of microbial activity which may enhance the transfer of OM to mineral surfaces and aggregates, fostering long-term stabilization (Mueller et al., 2017). In order to evaluate changing SOC dynamics of permafrost soils, we require a better understanding of the interactions between PyOM and SOC cycling within the soil and at the microscale and how these respond to continuous and discontinuous permafrost.

To investigate the vertical mobility and decomposition processes of PyOM and its precursor OM in permafrost-affected soils, we applied ^{13}C-labeled (2.9–4.4 atom%) ryegrass PyOM and OM (grass OM) in soil cores installed in the upper 10 cm of eleven boreal forest soil sites under continuous (northern sites) and discontinuous to sporadic (southern sites) permafrost conditions in Northern Canada. After two years of *in-situ* incubation, we aimed to: (i) Determine the decomposed and mobilized fractions of PyOM and OM, (ii) evaluate drivers of the PyOM and OM decomposition and mobility in bulk soils and its allocation in particle and density fractions, (iii) resolve how microscale organo-mineral interactions differ between PyOM and OM as well as permafrost conditions using nanoscale secondary ion mass spectrometry (NanoSIMS).

2. Material and methods

2.1. Study sites and soils

Eleven boreal forest sites were selected for the field incubation experiment, which was started in July and August 2019. The sites were located in the Boreal and Taiga Plain across the Northwest Territories and Alberta, Canada. They were divided into northern (N1–N5) and southern (S1–S6) sites, with around 1350 km distance between the two site regions. The northern sites were all under continuous permafrost conditions near the town of Inuvik with a high-subarctic ecoclimate (MAT: 9.5 °C and MAP: 200–300 mm). The southern sites were under discontinuous to sporadic permafrost in the South Slave Lake Region near Fort Smith with a sub-humid mid-boreal ecoclimate (MAT: 2 °C and MAP: 300–400 mm). Detailed site and soil descriptions are presented in Schiedung et al. (2022).

The soils at the northern sites were classified as Cryosols with turbic attributes at moist (mesic to subhygric, according to Johnstone et al. (2008)) sites N1–N3 and cambic/skeletic attributes at dryer (subxeric and subxeric to mesic) sites N4 and N5 according to the World Reference Base for soil resources (FAO (2014); Tables 1 and S1). The active layer depth (>0 °C and ice free during summer months), as determined during installation of the soil cores, ranged between 10 and 60 cm. The sites N1 and N2 represented flat lowland positions and the sites N4 and N5 represented flat elevated and exposed locations. Site N1 was located on the Great Bear Plain characterized by fine-textured glacial deposits. The sites N2–N4 were located on the Campbell Uplift, which is dominated by glacial till and colluvial deposits. The last northern site (N5) was located in the Mackenzie Delta Zone on an elevated position near Inuvik weather station.

Southern soils were classified as Regosols (S1, S2 and S5), Cambisols (S3 and S4) and one Luvisol (S1; Table 1) and no ice or cryoturbated features were observed in the upper 60 cm of these soils (Table S1). Site S1 to S3 were located along a landscape gradient towards the Pine Lake in the Wood Buffalo National park and together with S4 and S5 located in the Boreal Plain of the Slave River Lowlands dominated by sandy alluvial and eolian deposits. The site S6 was located at the transition of the Boreal to Taiga Plain and in the Hay River Lowlands, which are dominated by clayey lacustrine and glacial till.

2.2. Labeled material and experimental setup

Highly ^{13}C-labeled ryegrass (*Lolium perenne* L.) was produced using the Multi Isotope Controlled Environment (MICE) facility at the University of Zurich (Studer et al., 2017). The ryegrass was grown under a continuous 10 atom% enriched ^{13}C–CO_2 atmosphere. After around 20 days, the aboveground biomass was harvested and oven-dried at 40 °C. Ryegrass char, used as a proxy of PyOM, was produced by pyrolysis at 450 °C for 4 h under a N_2-atmosphere (Hammes et al., 2006). To obtain enough material, multiple individual growing batches were used. This resulted in one batch of grass OM and two batches of PyOM (Table 2).

Soil cores of 10 cm length and 6 cm diameter were installed in the upper mineral soils after carefully removing the organic layers, which ranged between 2 and 35 cm depth (Table 1). The soil cores included for all soils the A horizons (1–10 cm) and B-horizons (Table S1). The stainless-steel cores were installed by manual hammering to avoid disturbances of the soil cores. At each of the eleven forest sites, six locations (four for S6) were selected in a 30 × 30 m grid and in the near vicinity

Table 1
Site and soil properties. Site IDs, coordinates, soil types, average organic layer thickness (min to max range) of each site. Texture, soil organic carbon (SOC) contents, $\delta^{13}C$ of SOC, PyOM-C content determined by CTO-375, C:N ratio and pH are presented as site averages (±SE) in 0–15 cm soil depth as reported from soil pits studied Schiedung et al. (2022). The relative distribution of SOC in particulate organic matter (POM) and mineral associated fractions (>63 µm ($MAOM_{coarse}$) and <63 µm ($MAOM_{fine}$)) of control cores (without ^{13}C addition) in 0–3 cm soil depth, mean soil temperature over two years in 10 cm soil depth and site moisture classes. All soil horizons and depths are presented in Table S1.

Site	Latitude Longitude	Soil type (WRB)	Organic layer[a]	Texture[a,b]			SOC[a]	$\delta^{13}C$ of SOC[a]	PyOM-C_{CTO}	C:N[a]	pH_{CaCl}[a]	Proportion of fraction C on total C in 0–3 cm[c]			Mean soil temp. in 10 cm	Moisture class[d]
			[cm]	[%]			[%]	[‰]	[% on SOC]	[-]	[-]	[% of total SOC]			[°C]	
				Clay	Silt	Sand						POM	MAOM coarse	MAOM fine		
N1	68°02′32.0′′N 133°29′17.9′′W	Turbic Cryosol	13 (7–25)	25	50	17	6.44 (0.55)	−28.3 (0.1)	0.90 (0.05)	27.0 (2.0)	5.2	59	28	13	−0.4	Mesic to subhygric (3)
N2	68°10′07.5′′N 133°26′03.2′′W	Turbic Cryosol	14 (8–18)	30	52	14	4.57 (0.60)	−28.7 (0.1)	1.37 (0.12)	18.9 (0.7)	4.4	15	43	42	−2.3	Mesic to subhygric (3)
N3	68°10′11.7′′N 133°25′43.4′′W	Turbic Cryosol	11 (5–19)	27	44	26	3.23 (0.28)	−28.8 (0.1)	1.69 (0.15)	18.2 (0.6)	4.5	26	36	38	−1.2	Mesic (2)
N4	68°10′20.5′′N 133°25′26.4′′W	Cambic Cryosol	5 (2–10)	32	55	12	2.28 (0.14)	−29.2 (0.1)	2.90 (0.20)	18.5 (1.3)	3.6	48	33	19	−0.8	Subxeric (1)
N5	68°19′01.0′′N 133°31′57.2′′W	Skeletic Cryosol	5 (2–8)	25	58	15	5.05 (0.89)	−28.5 (0.1)	1.23 (0.09)	28.0 (1.4)	4.0	46	32	22	−2.4	Subxeric to mesic (2)
S1	59°31′31.9′′N 112°13′17.7′′W	Stagnic Regosol	24 (20–35)	3	14	82	1.46 (0.22)	−29.3 (0.2)	1.82 (0.26)	19.0 (0.9)	5.9	74	18	8	1.6	Mesic (2)
S2	59°31′29.5′′N 112°13′17.6′′W	Haplic Regosol	5 (3–10)	7	34	59	0.97 (0.08)	−29.8 (0.1)	2.37 (0.24)	14.4 (1.1)	4.6	45	38	18	1.9	Subxeric to mesic (2)
S3	59°31′27.5′′N 112°13′20.7′′W	Haplic Cambisol	5 (2–10)	5	29	65	1.36 (0.11)	−29.3 (0.1)	1.26 (0.15)	19.3 (0.8)	4.8	50	35	15	2.1	Subxeric to mesic (2)
S4	59°26′24.6′′N 112°21′12.2′′W	Haplic Cambisol	7 (3–12)	6	28	58	2.40 (0.74)	−29.0 (0.2)	2.34 (0.35)	17.7 (1.2)	6.8	49	30	20	3.0	Subxeric to mesic (2)
S5	60°01′02.2′′N 112°12′18.8′′W	Haplic Regosol	3 (2–5)	5	18	78	0.85 (0.09)	−30.0 (0.2)	1.61 (0.12)	24.1 (2.6)	5.5	62	27	11	3.7	Xeric (1)
S6	60°08′38.2′′N 113°38′55.5′′W	Leptic Luvisol	3 (2–3)	10	66	24	1.11 (0.18)	−30.2 (0.3)	2.21 (0.30)	16.6 (5.8)	5.2	66	17	17	3.8	Xeric (1)

[a] As presented in Schiedung et al. (2022).
[b] With clay (<0.002 mm), silt (0.002–0.05 mm) and sand (0.05–2 mm).
[c] Determined on control cores without PyOM and grass OM addition.
[d] Classified according to Johnstone et al. (2008) and summarized as (1) dry, (2) moist and (3) wet.

Table 2
PyOM and grass OM composition. Total C, $\delta^{13}C$ and C:N composition of the grass OM and PyOM batches used for the field incubation (± SE of analytical replicates).

Batch	Total C	$\delta^{13}C$	Atom%^{13}C	C:N[a]
	[%]	[‰]	[%]	[-]
Grass OM				
1.	40.9 (0.7)	3086 (32)	4.4	10.5 (0.1)
PyOM				
1.	46.1 (1.4)	1713 (31)	2.9	13.6 (0.8)
2.	49.7 (1.0)	2193 (38)	3.5	

[a] Means of four individual growing and pyrolysis batches.

(approx. 0.5–1.0 m distance) to soil pits studied in Schiedung et al. (2022). At each location one soil core was installed without any addition of ^{13}C OM (control core) and on the other two cores the labeled grass OM and PyOM was applied (total of 192 cores). The three treatments at each location were kept in a maximum distance of 30 cm to minimize spatial difference between treatments (Fig. S1). The elevated northern sites (N4 and N5) indicated permafrost related ground patterns in forms of polygon features. At these sites, the soil cores were installed in the center of larger polygons (e.g. 2 m width), similar to the soil pits studied in Schiedung et al. (2022).

A total amount of 327.6 ± 1.9 mg C was added to each core by applying 647.7 ± 2.4 mg PyOM and 846.1 ± 2.5 mg of grass OM. This corresponds to 109.6 ± 0.6 g C m^{-2} derived from PyOM and 122.3 ± 0.3 g C m^{-2} derived from grass OM and represents 10–30 years of natural PyOM inputs (Jones et al., 2019). The upper first centimeter of the soil in the core was carefully removed, the labeled material was added as an evenly distributed layer and the removed soil was carefully applied again (Fig. S1). The grass OM was cut into 1.0–1.5 cm long pieces prior to its application and PyOM was kept as produced. All soil cores were covered with a nylon mesh (2 mm mesh size) to avoid mass losses on the top. The cores were covered with the organic layer material in its initial horizontal sequence.

Temperature loggers (DS1922L-F5#, iButtonLink Technology, Whitewater, USA) were buried in 5 cm and 15 cm soil depth at the centered soil core location at each site (Fig. S2). At the southern sites (S1–S6) and two northern sites (N1 and N3), rooibos and green teabags were buried in 8 cm depth with four replicates following the protocol of the Tea Bag Index to study litter decomposition by mass losses (Keuskamp et al., 2013).

After two years (771 ± 3 days), all soil cores, temperature loggers and tea bags were sampled. For sampling, the organic layers were removed and after careful removal of the nylon-mesh, the cores were covered with tight vinyl caps on the top. Afterwards, the cores were carefully excavated and lifted out of the soil by closing the bottom with a trowel to avoid sample losses before closing it with a cap. All cores and teabags were stored at 3 °C in the dark prior to analyses.

2.3. Sample preparation

All soil cores were separated in 0–3 cm, 3–6 cm and 6–10 cm depth increments, while the upper 0–3 cm included the added labeled material (Fig. S1). The soils were sampled carefully from the top to avoid any cross-contamination with the labeled material. If the soil was lower in the core (maximum 1 cm for 16 cores), the actual soil surface was considered as top and the bottom layers reduced. After sampling, the soil core layers were dried at 40 °C to determine the dry mass. The material was homogenized by hand and an aliquot was sieved to 2 mm. Composites of the 0–3 cm layers (application layers) were obtained by equal weight of the sieved sample from each core of each site and treatment for SOC fractionation and micro-scale analysis.

2.4. Soil fractionation

Density and particle size fractionations were performed on 10 g of composite soil samples of the 0–3 cm depth increment per site and treatment. Free and light particulate organic matter (POM) was separated from the mineral soil with a density of 1.6 g cm^{-3} using a sodium polytungstate solution. The heavy mineral fraction was separated by size in a coarse mineral associated organic matter ($MAOM_{coarse}$) > 63 µm fraction and a fine mineral associated organic matter ($MAOM_{fine}$) < 63 µm fraction by wet sieving. Aggregate dispersion, such as ultrasonification, was not applied to avoid breakdown of PyOM particles. On average, 98 ± 1% of the initial mass and 97 ± 3% of total C were recovered. More details on the fractionation method are presented in the supplement.

2.5. Soil and organic matter analysis

All soil samples and fractions were milled and the total C and $\delta^{13}C$, relative to the international Vienna Pee Dee Belemnite (VPDB) standard, were obtained by using a dry combustion module cavity ring-down spectroscopy system (Picarro, Santa Clara, USA). Soils from the south contained inorganic carbonates as indicated by pH values around six (S1 and S4; Table 1). However, carbonates were not removed by acid treatment to avoid losses of labile C. The $\delta^{13}C$ values of the southern control soils indicated only little influence of carbonates (−28.9 ± 1.8‰ and a maximum of −16.9‰) but potential shifts were accounted for in the calculations by using the individual control core for each PyOM and grass OM treatment for the recovery calculations (Section 2.7).

Elemental composition of the initial PyOM and grass OM were determined by using dry combustion and high temperature pyrolysis (TruSpec Macro analyzer, Leco). Mid-infrared reflectance absorbance spectra were obtained in the range of 400–4000 cm^{-1} (average of 64 scans per sample at 4 cm^{-1} resolution) using Diffuse Reflectance Infrared Fourier Transformed (DRIFT) spectroscopy (TENSOR 27 spectrophotometer, Bruker, Fällanden, Switzerland). Background correction was performed using KBr, baseline corrections and corrections for water and carbon dioxide interferences were performed using OPUS (version 8.2) internal correction. The existing content of PyOM in the soils was determined on 0–15 cm soil depth from soil pits at the same sites (Schiedung et al., 2022) by using chemothermal oxidation (PyOM-C_{CTO}) following an adapted protocol presented by Agarwal and Bucheli (2011). Briefly, 40 mg of milled soil were combusted at 375 °C in silver capsules for 24 h under an O_2-atmosphere in an combustion oven followed by an acid fumigation presented by Walthert et al. (2010). All other soil parameters presented in Table 1 were determined at the same pits in 0–15 cm soil layers and are described in Schiedung et al. (2022).

2.6. Tracing the organo-mineral interactions of PyOM and grass OM at the microscale using NanoSIMS

Microscale analysis to trace ^{13}C derived from PyOM or grass OM, was conducted using nanoscale secondary ion mass spectrometry (NanoSIMS 50L, Cameca, Gennevilliers, France) on the $MAOM_{fine}$ (<63 µm) fractions of two exemplary sites from the northern (N2 and N4) and southern (S3 and S6) sites. We selected the sites according to representative soil properties with one site at moist and another one at dry soil conditions (Table 1). Of each selected site, 5–6 measurements were done for each PyOM and grass OM treatment.

For preparation, 2 mg of each $MAOM_{fine}$ were suspended in 10 ml deionized water and applied (20 µl) on GaAs wafer after dispersion for 1 min in a sonication bath. Scanning electron microscopy (SEM; Jeol JSM 5900LV, Tokyo, Japan) at 2 kV was used to identify regions of interest. Further details about measurement and settings are reported in the supplement.

A multi-channel machine-learning segmentation was used to analyze the NanoSIMS measurements (Schweizer et al., 2018; Inagaki et al.,

2020; Wilhelm et al., 2022). The raw data was corrected for electron multiplier dead-time using the OpenMIMS plugin in FIJI (Gormanns et al., 2012; Schindelin et al., 2015). To differentiate spatial patterns within the analyzed soil structures, supervised pixel classifications were performed by the machine-learning algorithm implemented in Ilastik 1.2 (Berg et al., 2019). A segmentation was done using the $^{16}O^-$, $^{12}C^- + ^{13}C^-$, $^{12}C^{14}N^-$ to differentiate OM (high C^- and high CN^-), mineral regions (high O^-), and the background (low ion counts). The differentiation of ^{13}C-enriched spots was done in a separate step using the ^{13}C enrichment ratio calculated as $^{12}C^{13}C^-:(C^{12}C^- + ^{12}C^{13}C^-)$ with a contrast enhanced between 0 and 4.5%. The segments were cross-checked based on distinct CN:C ratio and ^{13}C enrichment. The total area of measured particles was 10,356 μm^2.

2.7. Calculations and statistical analysis

The recoveries of ^{13}C derived from C of added PyOM (PyOM-C) and grass OM (grass-C) in the bulk soils and fractions were calculated using the ^{13}C atomic fractions as recommended by (Coplen, 2011) and calculated as:

$$m_{recovery_{13_C}} = \frac{xE(13_{C\,sample}}{xE(13_{C\,initial}} \times m_{sample} \quad (1)$$

where $xE(13_{C\,sample}$ and $xE(13_{C\,initial}$ are the excess isotope-amount fraction of the sample and corresponding initial grass OM and PyOM (Table 2) and m_{sample} is the total mass of C of the sample in [mg]. Further details are presented in the supporting information. The total recovery of grass- and PyOM-C in the soil cores was calculated as the sum of ^{13}C found in the three depth layers per core.

At three core locations, the ^{13}C recovery of cores with PyOM addition was too high (e.g. >115%), which can be attributed to variability of the labeled material or not accountable errors in the field or sample handling. Thus, these three core locations were excluded from further analyses (one location at site S1, S4 and S6).

To identify site and soil properties controlling the recovery of grass-C and PyOM-C, Principal Component Analysis (PCA) were performed using the *prcomp* function and the *factoextra* package (Kassambara and Mundt, 2020) for visualization of PCA parameters and results using R Studio (Version 1.3.1073; R Core Team (2021)). All considered site and soil specific parameters are presented in Table 1 and Table S4. Pre-analysis revealed a separation of northern and southern sites by the PCA (Fig. S3). Therefore, further PCAs were conducted individually for northern and southern sites. The PCAs were performed with all site and soil specific parameters (active variables), scaled to unify variances, and the coordinates of PyOM- and grass-C recoveries were predicted (quantitative variables) in the individual PCA.

Differences in total recovery of PyOM- and grass-C and in individual core depths were tested using analysis of variances (ANOVA) with computing p-values on a 95% family-wise confidence level and post-hoc Tukey significance difference of means using Bonferroni adjustment using the *multcomp* package (Hothorn et al., 2021). Differences between PyOM and grass OM treatments or cumulated between northern and southern sites were tested using two sample Student's t-tests. Normal distribution and homogeneity of variances were tested using Shapiro-Wilk and Levene tests and data transformation was applied to reach criteria (e.g. log- or square-root-transformation). Non-parametric Pairwise Wilcoxon Rank Sum Tests and two-sample Wilcoxon tests were performed if criteria of normality and variance homogeneity were not fulfilled. All data is presented as means of the field replicates and with standard error of the mean (SE) if not stated differently.

3. Results

3.1. Site properties and field variability

The total C contents and C:N ratios were generally higher at northern sites compared to southern sites (Table 1). For most of the sites, the total C was highest in 0–3 cm and decreased with core depth (Figs. S4 and S5). The finer-textured northern soils contained up to 20% less POM as a fraction of total C in the upper 0–3 cm than the southern soils (Fig. S6 and Table 1). The two MAOM fractions together ($MAOM_{coarse}$ and $MAOM_{fine}$) contained up to 80% of total C at sites N2 and N3. Higher C contents at northern sites resulted in higher absolute amounts of C present as POM compared to southern soils (Fig. S7).

The spatial variability of bulk C between the cores was high, even with the closest possible vicinity between cores (30 × 30 cm; Fig. S1). Large total C contents (>10%) at some sites (e.g. N1, N4, S1 and S4) indicated that the upper 10 cm of the mineral soils might have been influenced by indistinct transitions of organic layers and mineral soils (Figs. S4 and S5). For all sites, the variability in total C exceeded 30% between treatments (Fig. S8) and it was even larger (up to 45–54%) for the control cores as averages of all depths (Fig. S9). The $\delta^{13}C$ of control cores showed less variability (2–4%), with higher variation in soils with carbonates at southern sites (Fig. S10). The substantially lower field variability of $\delta^{13}C$ confirms that the isotopic compositions of control cores are representative to trace the ^{13}C-labeled PyOM and grass OM by isotopic recovery calculations.

3.2. Recovery and loss of PyOM- and grass-C

The total recovery of PyOM-C revealed substantial losses after two years at northern sites of 39 ± 6% and thus more than three times larger losses than at southern sites (11 ± 4% loss; Fig. 1a and Table S2). The grass-C recoveries were generally lower than the PyOM-C recoveries, indicating losses of 69–84% with larger losses at southern sites.

The individual sites showed no significant differences in the total recovery of initial PyOM- or grass-C when considering only northern sites (Fig. 1b and Table S3) and southern sites (Fig. 1c and Table S4). Two northern sites (N3 and N5) indicated similar PyOM-C and grass-C recoveries (Table S5).

In the soil cores, the majority of initial PyOM-C (north = 55.2 ± 5.0%; south = 83.8 ± 3.9%) and grass-C (north and south around 20%) remained in the upper 0–3 cm (Fig. 1b and c and Table S2). With core depth, the recoveries of initial PyOM- and grass-C were similar for northern and southern sites in 3–6 cm depth (Table S2). In the lowest core layers, a larger proportion of initial PyOM was recovered in northern soils (north = 1.9 ± 0.4% and south = 1.0 ± 0.3%), while grass-C recoveries were similar for northern and southern sites (on average 0.4 ± 0.1%).

3.3. Litter decomposition and mass losses

Green tea litter (more labile OM) mass losses were larger compared to the rooibos tea litter (more recalcitrant OM) in all soils after two years of incubation (Fig. 2). Remaining green tea litter masses were significantly lower in northern soils by around 10% compared to southern soils, while around 20% less rooibos tea litter remained in the southern than in northern soils (Table S2).

3.4. Distribution of PyOM and grass OM in fractions

The majority of remaining PyOM-C (around 60%) was recovered in the POM fractions after the two years of incubation at northern and southern sites (Fig. 3). For northern and southern soils, similar proportions of recovered PyOM-C were mineral associated, with around 20% of recovered PyOM-C in the $MAOM_{fine}$ fractions alone (Fig. 3).

At the northern sites, around half of the recovered grass-C was in the

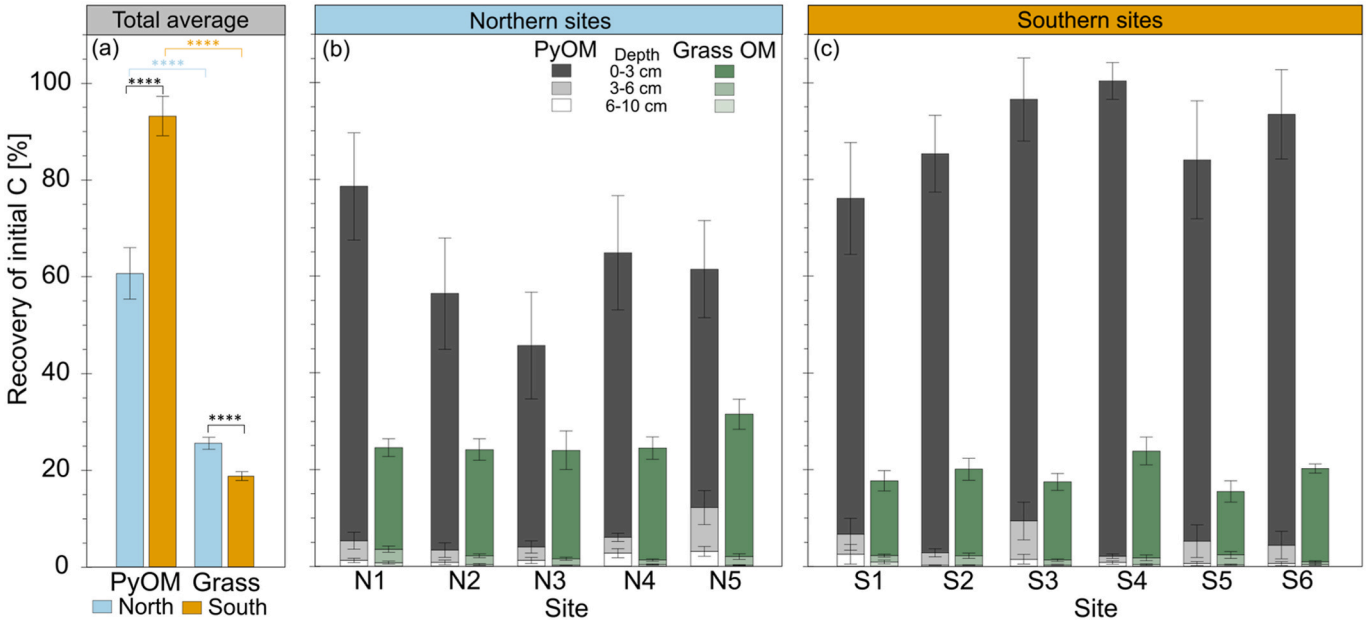

Fig. 1. Recovery of PyOM and grass OM in soils. Total recovery of initial PyOM- and grass-C with significance ($p < 0.001$) indicated by asterisk (a) and recovery of initial with depth for northern (b) and southern (c) sites. All recoveries are presented in Table S2. Significances of differences between PyOM- and grass-C recoveries between sites are shown in Tables S3 and S4 and between PyOM and grass OM with depth in Table S5. Error bars indicate the standard error of the mean of replicates per site.

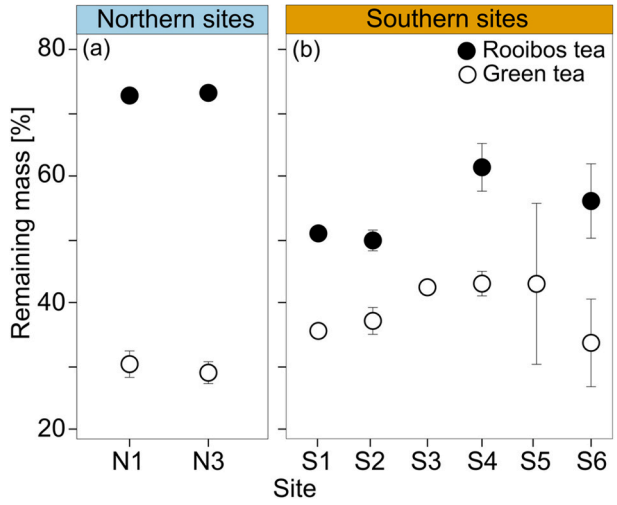

Fig. 2. Teabag litter recoveries. Remaining mass of green tea (labile OM) and rooibos tea (more recalcitrant OM) litter after two years of in-situ incubation in 8 cm soil depth for northern (a) and southern (b) sites with standard error of the mean of 3–4 replicates per site. All recoveries are presented in Table S2.

POM fractions (Fig. 3a). The distribution of recovered PyOM- and grass-C across all fractions was similar at northern sites with only larger differences at N2. At the southern sites, more than two-thirds of recovered grass-C was located in the mineral fractions with the largest recovery in the $MAOM_{coarse}$ fraction (Fig. 3b).

3.5. Microscale PyOM and grass OM dynamics

The analysis of the $MAOM_{fine}$ fraction by SEM and NanoSIMS revealed the allocation of ^{13}C from PyOM or grass OM within distinct microscale structures through organo-mineral interactions. The PyOM was retained as fragmented particles, while the ^{13}C derived from grass OM was found to be associated with mineral surfaces (Fig. 4, further images at S13 and S14). Individual PyOM particles in northern soils indicated partial co-localization with mineral surfaces (Fig. 4e1) or PyOM was found on mineral surface as ~1 μm-sized spots (e.g. Fig. S13a, b and e). The grass OM derived ^{13}C was found to be much more dispersed across the mineral surfaces (e.g. Fig. 4d4-e4 and Fig. S14) at southern sites compared to northern sites, where only few and larger ^{13}C-enriched spots were found (Fig. 4d2-e2 and Fig. S13). Image analysis based on all images (4473 μm^2 of sample surface at northern sites, 1668 μm^2 at southern sites) showed that the organic matter coverage of the mineral surface was larger at southern sites (24 ± 1%) compared to northern sites (11 ± 2%; Fig. S15).

3.6. Site and soil properties controlling PyOM-C and grass-C recoveries

At the northern sites, PyOM- and grass-C recoveries were higher in soils with a larger proportion of POM, higher C:N and a larger proportion of aliphatic to aromatic compounds of the SOC (Fig. 5a). On the same dimension, higher recoveries were projected with higher total Fe, Al and silt contents. The recoveries of PyOM- and grass-C were higher when total mineral associated SOC ($MAOM_{fine}$ and $MAOM_{coarse}$) and sand content were low. The total SOC contents as well as PyC_{CTO} contents, together with most other parameters, had little influence (second component) on the recovery of PyOM- and grass-C. The PyOM-C recovery was projected with the soil's C:N and grass-C recovery with the relative proportion of aliphatic and aromatic SOC composition.

At the southern sites, PyOM- and grass-C recoveries were closely projected to each other and generally higher when the SOC proportions in $MAOM_{fine}$ and PyC_{CTO} contents were higher (Fig. 5b), which was especially the case for PyOM-C recoveries. Recoveries of PyOM- and grass-C were higher at sites with low C:N, less SOC present in the POM fraction and a higher proportion of cellulose to lignin.

4. Discussion

4.1. Loss of fresh PyOM and OM and related controlling factors

Permafrost-affected soils showed large losses of fresh PyOM and non-pyrolyzed grass OM after two years of *in-situ* incubation and thus quick

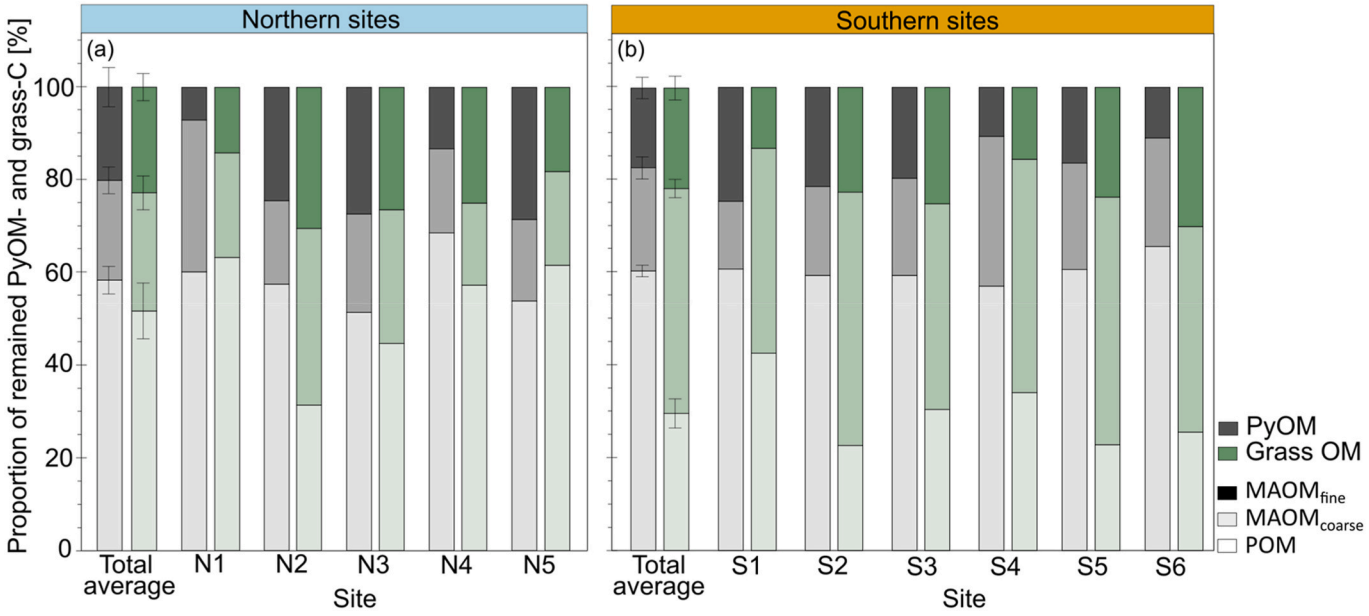

Fig. 3. Allocation of PyOM and grass OM in fractions. Remaining PyOM- and grass-C in particulate organic matter (POM) and coarse mineral associated organic matter ($MAOM_{coarse}$) and fine mineral associated organic matter ($MAOM_{fine}$) fractions in the upper 0–3 cm of the cores for northern (a) and southern (b) as average of all sites and for individual sites.

responses to fresh OM (Figs. 1 and 2). With more than one-third of loss, the PyOM losses were unexpectedly larger at northern sites under continuous permafrost than at southern sites under discontinuous to sporadic permafrost conditions (Fig. 1a). The losses of grass OM were larger but vice versa than for PyOM with larger losses at southern sites. This indicates decoupled mechanisms for PyOM and non-pyrolyzed grass OM losses. In addition to the direct tracing of ^{13}C-labeled PyOM- and grass-C, the tea litter decomposition (mass losses) indicated further differences in the cycling of fresh OM in permafrost-affected soils (Fig. 2). Decomposition of labile green tea were significantly larger at northern sites compared to southern sites, while slow cycling rooibos tea litter was less decomposed at northern sites. These losses of non-pyrolyzed OM are in the range of reported recoveries of fescue grass litter (32 ± 2%) and woody tissue (72 ± 4%) after six years of above-ground field exposure across Canada (Trofymow et al., 2002). In a global comparison, Djukic et al. (2018) reported green tea mass recoveries of approx. 30–40% and rooibos tea litter masses of around 70% after a maximum of 36 months for boreal and arctic regions, which is comparable to our results except of higher mass losses of rooibos tea litter at southern sites (53 ± 2% recovered mass). The large losses of PyOM, grass OM and teabag litter after two-years in this study, highlight a potential rapid OM cycling in permafrost-affected forest mineral soils on a relative short timescale of two years even under continuous permafrost conditions depending on the composition of the fresh OM.

Permafrost-affected soils are reported to contain mainly unprocessed OM (Ping et al., 2015), as found in the northern soils in this study (Schiedung et al., 2022) with high POM proportions (Table 1 and Fig. S7; 39–58% of total SOC). These large amounts of potentially labile OM would provide sufficient substrate for microbial decomposition (Mueller et al., 2015; Ping et al., 2015). However, the microbial activity in permafrost-affected soils is limited due to the low temperatures but also a limited accessibility of N and other nutrients in the present OM (Kaiser et al., 2007; Sistla et al., 2012; Wild et al., 2013; Schuur et al., 2015). Therefore, available N in fresh litter and OM rather than the additional C, acting as an energy source for the microbial community, was reported to be a main factor controlling its decomposition in high-latitude boreal (Berg and Ekbohm, 1991) and tundra soils (Wild et al., 2014, 2016).

The total PyOM-C recoveries within the 10 cm soil cores were projected along the soil C:N ratios of the northern and southern soils in the PCA and losses were larger when bulk soil C:N ratios were lower in northern soils (Fig. 5). The loss of PyOM-C in northern soils could be related to a co-metabolism of C to access available N and consequently act as a N source for the microbial community. As an example, site N3 had bulk soil C:N ratios of 18.2 and showed the largest loss of PyOM-C (45.2 ± 12.6% recovered initial PyOM-C; Table 1 and Fig. 1). The losses of grass OM and green tea litter (C:N of 12.2 ± 0.1, Keuskamp et al., 2013), both with low C:N ratios, were also high at this site (Fig. 2). In comparison, the rooibos tea litter with a high C:N ratio (42.9 ± 1.8, Keuskamp et al., 2013) may not have provided accessible N, resulting in smaller losses in northern soils. Compared to the labeled PyOM and grass material applied in 0–3 cm, the teabags were installed in 8 cm soil depth. The green tea especially indicated large mass losses in northern soils. This indicates a large decomposition potential even in larger soil depth when the OM contains sufficient N. It needs to be considered that we used site specific C:N ratios for our analysis here (Table 1), which were determined in 0–15 cm soil depths in pits sampled in close vicinity of the soil core locations (e.g. <1 m; Schiedung et al., 2022). Therefore, depth specific small-scale differences in C:N due to soil horizons (Table S1) are not taken into account, which might affect the losses by mineralization with soil depth in the cores. However, our findings indicate that fresh OM and chemically more persistent PyOM may act as an available nutrient source resulting in a co-metabolism of C and rapid mineralization in permafrost soils.

The biotic oxidation of PyOM by fungi (Czimczik and Masiello, 2007; Gibson et al., 2016) might enhance N availability similarly observed for polymeric compounds, including lignin (Koranda et al., 2014), and also polyaromatic compounds (Lehmann et al., 2011). Fungal activity is found to be a substantial driver of OM cycling in boreal forest soils (Holden et al., 2013). Additionally, PyOM can enhance the N cycling in soils and N containing heterocyclic compounds originated from PyOM can be degraded microbially (Maestrini et al., 2014; Hilscher and Knicker, 2011a). The direct uptake of N derived from PyOM by plants and soil microbial community was found in permafrost-affected tundra soils within two years of *in-situ* incubation using ^{15}N labeled PyOM (Xu et al., 2022). This supports that PyOM can function as a significant nutrient source in permafrost-affected soils. Physical breakdown through freeze-thaw dynamics may have reduced the particle size and

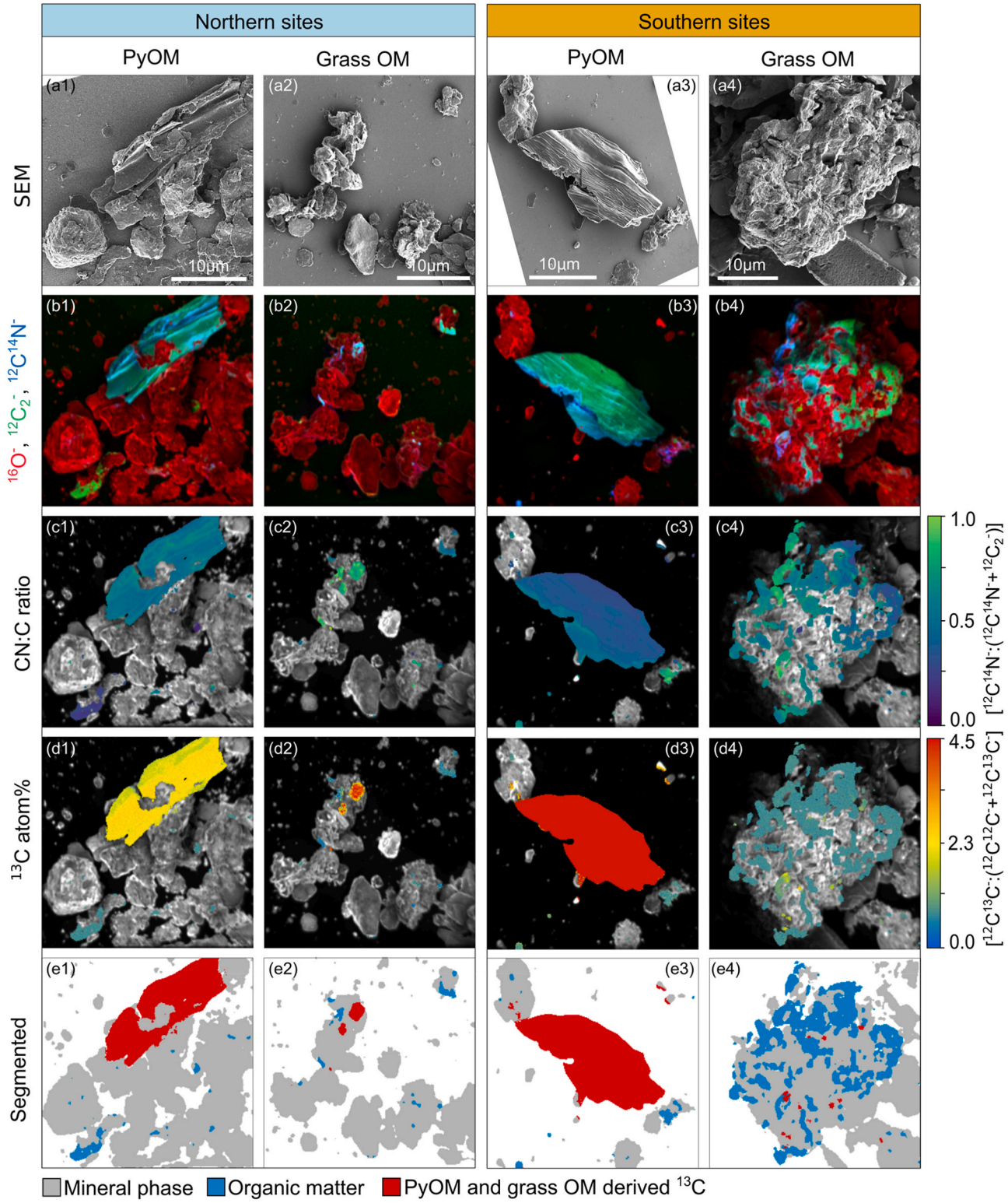

Fig. 4. Microscale distribution of PyOM and grass OM. Microscale analysis of the $MAOM_{fine}$ (<63 µm) fractions for northern and southern soils with PyOM and grass OM addition shown as exemplary images. Scanning electron microscopy images (a1-a4) and NanoSIMS composite images of $^{16}O^-$ (red), $^{12}C_2^-$ (green) and $^{12}C_{14}N^-$ (blue) secondary ion counts (b1-b4), CN:C ratio (c1-c4); atomic fraction of ^{13}C (d1-d4) and segmented composition separated in mineral phase, initial OM and C derived from ^{13}C-labeled PyOM or grass OM (e1-e4). Example images from the sites N2, N4, S3 and S3, respectively. Further images are in the supplement (Fig. S13 for northern sites and Fig. S14 for southern sites).

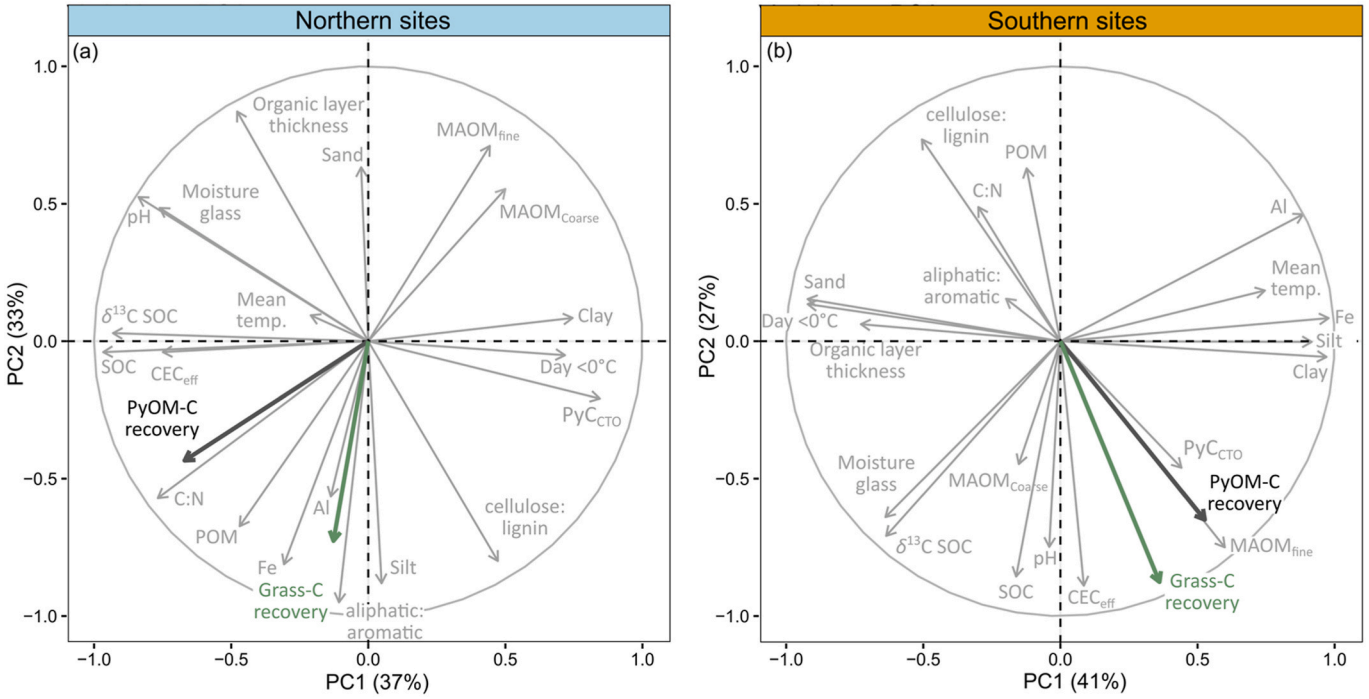

Fig. 5. Controlling factors of PyOM and grass OM recoveries. Principle component analysis with soil and site properties (Table 1 and S6) with active variables to construct the PCAs (grey arrows) and predicted PyOM- and grass-C recovery for northern (a) and southern (b) sites.

increased the surface area of PyOM (Spokas, 2010; Pignatello et al., 2015). This would further expose PyOM to microbial and fungal degradation as well as abiotic oxidation and contribute to large losses in the northern soils.

The southern sites were reported to contain larger proportions of already processed OM as indicated by its isotopic composition, lower C:N ratios and depletion in aliphatic and cellulose like compounds compared to the northern soils (Table 1 and S6; Schiedung et al. (2022)). The PCA analysis suggested that PyOM- and grass-C recoveries are driven by more similar controlling factors at southern sites than at northern sites, indicating a rather energy limited system (Fig. 5). Therefore, the higher PyOM stability could be explained with its inherent persistence to degradation due to its aromaticity in the southern soils where nutrient availability is not limited as in continuous permafrost affected soils in the north.

The cycling of PyOM in soil can enhance or reduce native SOC decomposition (priming effect), which may affect the total soil C balances (Abiven and Andreoli, 2011; Maestrini et al., 2015; Pluchon et al., 2016). Further, PyOM can have a physico-chemical effect on the native SOC cycling by enhancing its desorption from mineral surfaces due to a higher sorption affinity and thus release more degradable and already sorbed OM from soils (Kaiser and Guggenberger, 2000; Schiedung et al., 2020). We found large spatial variability between our treatment soil cores installed in close vicinity (i.e. 30 × 30 cm; Fig. S9). The large variability in total C did not allow to disentangle changes in the native OM decomposition caused by PyOM and grass OM addition since native and present SOC changes were within the observed spatial variability between the treatment cores at each sample location (Fig. S11). Our findings highlight that *in-situ* priming effects and PyOM interactions with native SOC are challenging to trace even when highly ^{13}C-labeled OM and a high number of field replicates is used due to pronounced spatial variability of SOC in boreal forest mineral soils.

Our results support that PyOM stability in soils is not exclusively controlled by its chemical and physical properties but depends highly on site specific soil properties (Czimczik and Masiello, 2007; Abney et al., 2019) and does not follow systematically fresh non-pyrolyzed OM and litter dynamics. Particularly, permafrost conditions and related microbial activity as well as nutrient conditions could affect the PyOM stability. However, permafrost thawing due to global warming will change the composition, diversity and activity of the microbial community (e.g. bacterial to fungal biomass). How this will affect SOC cycling, including decomposition of PyOM, and nutrient availability is largely unknown (Peplau et al., 2021; Ernakovich et al., 2022; Rijkers et al., 2022; Scheel et al., 2022). When comparing our sites under continuous permafrost to those under discontinuous to sporadic permafrost, the PyOM persistence may increase in the future when the decomposition of non-pyrolyzed OM and nutrient availability increase with permafrost thaw and warming.

4.2. Mobility and translocation of PyOM and grass OM

Vertical PyOM- and grass-C incorporation into lower soil depths after two years of *in-situ* incubation was limited. Most of the remaining C was recovered in the upper 0–3 cm core layers (>90% of recovered C; Fig. 1 and Table S2). Deeper translocation of PyOM- and grass-C was in northern and southern soils on much smaller magnitude than the previously discussed losses. Low recoveries of initial PyOM- and grass-C in 6–10 cm core depth of 0.2–3% indicated that deeper translocation to soil depth >10 cm may have been minor during two years.

The vertical mixing by cryoturbation and related freeze-thaw dynamics are important controlling factors of C distribution in permafrost and ice-rich soils (Ping et al., 2015). The northern soils in this study stored up to 70% of the total SOC stocks in 15–60 cm depth compared to the southern soils where around 60% of the total SOC was in the upper 0–15 cm depth, highlighting the importance of vertical mixing by cryoturbation at the study sites (Schiedung et al., 2022). Mean soil temperatures over the two years of the experiment were lower in the northern soils (−2.4 to −0.4 °C in 10 cm) compared to the southern soils (1.6–3.8 °C in 10 cm; Table 1 and Fig. S2). At northern sites, periods of temperatures fluctuating around 0 °C during spring and autumn (zero curtain-effect) were longer than at southern sites. Further, 50% of the experimental time were below 0 °C in 10 cm soil depth at the north (Table S6). Thus, freeze and thaw dynamics were probably more intense in the northern soils over two years of the experiment. The recoveries of

PyOM- and grass-C below the application layer (0–3 cm), however, were not significantly higher at northern compared to southern sites. Therefore, cryoturbation was not substantially contributing to vertical translocations of PyOM and grass OM after two years. However, the cambic and skeletic Cryosols (N4 and N5) showed on average up to three times larger PyOM-C recoveries in the two deeper core layers (3–6 cm and 6–10 cm) compared to the other northern sites (Fig. 1a and Table S2). These two sites were located on exposed and elevated landscape positions, which were characterized by shallow organic layers. This limits potential insulation effects (Table 1) and results in fast seasonal changes in soil temperature and freeze-thaw dynamics (Table S6). The physical stability of PyOM is lower compared to the initial un-pyrolyzed OM as a result of condensation reactions (Pignatello et al., 2015). Physical pressure by expansion and shrinking during freeze and thaw can break the PyOM down in smaller particles, which will ultimately determine its mobility and vertical translocation in soils (Spokas et al., 2014; Lehmann et al., 2015). Therefore, physical breakdown and fragmentation of PyOM could have been more pronounced at the exposed sites (N4 and N5) compared to the less exposed and more insulated sites (N1–N3, Table 1 and S5), leading to an increased vertical translocation.

The vertical translocation of PyOM in soils can take place as dissolved or colloidal transport with percolating water (Wagner et al., 2017, 2018) and as particles (Hobley, 2019). In comparison, inputs of C derived from non-pyrolyzed OM litter into soils, such as grass OM in our study, are transported vertically as dissolved organic C (Kalbitz et al., 2000; Kaiser and Kalbitz, 2012). Batch experiments (Abiven et al., 2011), saturated column experiments (Hilscher and Knicker, 2011b; Schiedung et al., 2020) and field experiments (Major et al., 2010; Maestrini et al., 2014) showed that the transport of PyOM in dissolved and colloidal form represents only <1% of the total PyOM. This transport mainly occurs with the first flush, mobilizing initially soluble PyOM fractions or occurring with aging of the PyOM. Under field conditions, Singh et al. (2014) reported that 3–4% of applied wood PyOM in a temperate forest soils moved below the application layer after ten months. We found recoveries of 2.1–12.1% of applied PyOM mobilized and retained at 3–10 cm soil depth. These higher recoveries might indicate that the vertical PyOM transport in soils under field conditions, including cryoturbation and seasonal soil moisture changes, is likely to be controlled by translocation of particles.

Particulate transport results in a heterogeneous input of PyOM with depth, which is indicated by a much larger variability in recoveries compared to the recovered grass-C (Fig. 1 and Table S2). Given no significant differences between and within northern and southern sites and considering the large range of soil properties (e.g. clay content 3–32%, sand content 12–82% and pH 3.6–6.8; Table 1), vertical translocation of PyOM can be similar in terms of its quantities after two years under field conditions in boreal forest soils but with a high spatial variability on relatively small scales (i.e. 30 × 30 m plot). This challenges an accurate large-scale quantification of PyOM under field conditions due to its spatial variability as a result of distinct and small-scale controlling factors of PyOM mobility in soils, which would be even more pronounced considering its highly variable input by natural wildfire.

After a natural wildfire, PyOM first remains on the soil surface and is therefore initially controlled by lateral transport on the soil surface (Rumpel et al., 2015; Masiello and Berhe, 2020; Bellè et al., 2021), drivers we could not reproduce in this experiment. However, our approach allowed the comparison of the vertical mobility of PyOM and its precursor grass OM. Even though only a few sites indicated significant higher amounts of recovered PyOM-C in deeper soil core layers (Table S5), our results showed a tendency towards higher recovery of PyOM-C compared to grass-C with soil depth at northern and southern sites (Fig. 1, Table S5). This is in agreement with increasing proportions of PyOM-C on the total SOC with soil depth in temperate and boreal forest soils (Soucémarianadin et al., 2014, 2019). An increasing fraction of PyOM in greater soil depth is attributed to the higher persistence of PyOM compared the non-pyrolyzed OM (Bird et al., 2015), such as the grass OM here, which will be exposed to degradation during its vertical transport (Don and Kalbitz, 2005; Tipping et al., 2012). The continuous downward migration of PyOM can be linked to the seasonally decoupled (Hockaday et al., 2007; Wagner et al., 2017) and consistent export of PyOM from soils to the aquatic system (Dittmar et al., 2012; Ding et al., 2013), controlling the C cycle of fire-affected ecosystems.

4.3. Allocation of PyOM and grass OM in fractions and on microscale

The recovered PyOM was highly associated to the mineral fractions with up to 40% of the remaining PyOM across northern and southern sites (Fig. 3). The significantly higher losses at northern compared to southern sites (Fig. 1) did not affect the relative distribution of remaining PyOM within soil fractions. This demonstrates that abiotic interactions, such as sorption and aggregation, controlled the allocation of PyOM within soil fractions over two years.

Mineral-PyOM associations can be favored by direct interactions of functional groups of PyOM with clay minerals or reactive Fe/Al-(oxy-hdro)oxides (Joseph et al., 2010; Pignatello et al., 2015). A rapid association of PyOM with the mineral fractions was found in experimental set-ups excluding biological degradation processes with up to 40% of vertically transferred PyOM associated to the mineral fractions in a loamy Luvisol (Schiedung et al., 2020). Singh et al. (2014) recovered >25% of PyOM added to a temperate forest soil occluded in the mineral fractions after ten months of incubation. Brodowski et al. (2006) found up to 24% of the total PyOM in forest soils to be associated and occluded in the mineral fractions. Ponomarenko and Anderson (2001) found young and hydrophobic PyOM in the fine fraction <50 μm as single particles, while older PyOM was found in the sand size fractions (50–2000 μm) and coated with clay minerals in a Black Chernozem in Saskatchewan, Canada. This highlights that PyOM is mainly present as particles in mineral soil fractions and can act as binding agent for aggregates. Our microscale analysis of the clay and silt size fractions ($MAOM_{fine}$), using SEM and NanoSIMS imaging, indeed revealed that mainly PyOM particles were recovered (Fig. 4, S13 and S14). The PyOM at northern sites showed more interactions and direct mineral coating (Fig. 4 a1-e1) and partially larger recoveries of PyOM-C on surfaces of larger aggregates not resembling PyOM morphologies (Fig. S13) compared to the southern sites. This supports that the PyOM was altered by microbial processes in continuous permafrost-affected northern soils, which have increased its general mineral interaction.

The grass OM incubation revealed larger differences between northern and southern sites as indicated by the grass OM recovery compared to the PyOM recovery (Fig. 3). At the southern sites, a much larger proportion of grass-C was associated with the mineral fraction compared to the northern sites. The general losses, however, were high for both permafrost regions (Fig. 1). Therefore, microbial processing of fresh OM resulted in a more extensive allocation towards mineral fractions in southern soils under discontinuous to sporadic permafrost conditions, while under continuous permafrost conditions in the north, fresh grass OM was retained as POM. However, at the lowland site N2 a larger proportion of grass-C remained in the mineral fractions on a similar magnitude than the southern soils (around 70% of remained grass-C). Mineral associated OM in permafrost- and cryoturbation-affected soils was found to contain up to 64% of the total SOC (Gentsch et al., 2015a), which is in accordance with our results (Fig. 3 and Table 1). Furthermore, it is reported that the MAOM fraction may have a higher bioavailability than POM in cryoturbated soils (Gentsch et al., 2015a, 2015b). The continuous and fine textured permafrost-affected soils with predominantly free mineral surfaces in the clay and silt size fraction (Fig. S15) may therefore have an increased potential to stabilize OM on mineral surfaces when pedoclimatic conditions change with warming (Gentsch et al., 2015b; Mueller et al., 2017).

The microscale analysis of the $MAOM_{fine}$ fractions revealed a larger distribution of small grass-C patches on aggregate surfaces and lower ^{13}C

label at southern sites (Fig. 4 a4-e4 and S14) compared to larger spots and more concentrated recoveries at northern sites with high ^{13}C label, close to the initial label (Fig. 4 a2-e2 and S13). This indicates that grass OM was affected by physicochemical stabilization by mineral surfaces and aggregation, which could favor the creation of microbial hotspots (Mueller et al., 2015). This would contribute to a higher microbial accessibility of the MAOM C under continuous permafrost conditions. At the southern sites, grass OM might be stabilized after microbial degradation resulting in a long-term stabilization similar to observations and conceptualizations as for temperate soils (Lützow et al., 2006; Kögel-Knabner et al., 2008; Kleber et al., 2021). This underlines that the organic C cycle of continuous permafrost-affected soils differs from our current understanding mainly based on temperate soil observations and long-term stabilization mechanisms are not solely controlled by mineral interactions.

5. Conclusions

Forest soils affected by continuous permafrost showed three times larger losses of PyOM compared to soils under discontinuous to sporadic permafrost. This makes the PyOM persistence a function of soil (e.g. nutrient availability) and landscape (e.g. permafrost intensity) properties, which can be counter intuitive in permafrost-affected soils. The losses of PyOM followed different mechanisms than non-pyrolyzed OM losses: Its decomposition can be more associated to physical fragmentation by freeze-thaw dynamics, which reduces particle sizes and potentially increases nutrient availability, favoring its decomposition and its vertical mobility in continuous permafrost affected soils. Vertical translocation of PyOM, predominantly as particles, was limited and decoupled from permafrost conditions after two years. Allocation of PyOM towards mineral fractions is important for its fate in soils (~40% of remaining PyOM associated) and can also be independent of permafrost conditions. Non-pyrolyzed grass OM cycling and mineral association was more pronounced under discontinuous to sporadic permafrost. Our results highlight that permafrost-affected boreal forest soils are sensitive to fresh PyOM and OM, resulting in its decomposition. The responses can be decoupled between PyOM and non-pyrolyzed OM and differ from soil C dynamics knowledge based on temperate soil observations. The cycling and its controlling mechanisms of PyOM and non-pyrolyzed OM in soils might change with changing climatic and environmental conditions.

Authors contribution

SA acquired the funding. MS, SLB and SA conceptualized the fieldwork. MS and SLB conducted the fieldwork. MS conducted laboratory work for bulk and fraction analysis. CH and SAS prepared and conducted SEM and NanoSIMS analyses together with MS. MS, SAS and SA analyzed the data. MS wrote the manuscript with contribution of all authors and all authors approved the final manuscript.

Declaration of competing interest

The authors declare that they have no known competing financial interests or personal relationships that could have appeared to influence the work reported in this paper.

Data availability

The data related to this manuscript are available at https://doi.org/10.5281/zenodo.6992753.

Acknowledgement

This work was supported by the Swiss National Science Foundation [grant no. 200021_178768]. We gratefully acknowledge the support and assistance of the community of the Northwest Territory Métis Nation in Fort Smith, the Wood Buffalo National Park (WBNP) and the Aurora Research Institute (ARI) during the field work and installation of the soil cores. We gratefully thank the fieldwork team and technical staff of Environmental Natural Resources (ENR) in Fort Smith, the WBNP and ARI for their extraordinary support and sampling of all soil cores, without which we would have not been able to conduct this study during the SARS-CoV-2 pandemic. We thank Nadja Hertel for assistance during sample preparation, Gertraud Harrington for technical assistance at the NanoSIMS, Rahel Wanner for CHN–O analyses and Carsten W. Müller for data discussion.

Appendix A. Supplementary data

Supplementary data to this article can be found online at https://doi.org/10.1016/j.soilbio.2023.108959.

References

Abiven, S., Andreoli, R., 2011. Charcoal does not change the decomposition rate of mixed litters in a mineral cambisol: a controlled conditions study. Biology and Fertility of Soils 47, 111–114. https://doi.org/10.1007/s00374-010-0489-1.

Abiven, S., Hengartner, P., Schneider, M.P.W., Singh, N., Schmidt, M.W.I., 2011. Pyrogenic carbon soluble fraction is larger and more aromatic in aged charcoal than in fresh charcoal. Soil Biology and Biochemistry 43, 1615–1617. https://doi.org/10.1016/j.soilbio.2011.03.027.

Abney, R.B., Jin, L., Berhe, A.A., 2019. Soil properties and combustion temperature: controls on the decomposition rate of pyrogenic organic matter. Catena 182, 104127. https://doi.org/10.1016/j.catena.2019.104127.

Agarwal, T., Bucheli, T.D., 2011. Adaptation, validation and application of the chemothermal oxidation method to quantify black carbon in soils. Environmental Pollution 159, 532–538. https://doi.org/10.1016/j.envpol.2010.10.012.

Bellè, S.-L., Berhe, A.A., Hagedorn, F., Santin, C., Schiedung, M., van Meerveld, I., Abiven, S., 2021. Key drivers of pyrogenic carbon redistribution during a simulated rainfall event. Biogeosciences 18, 1105–1126. https://doi.org/10.5194/bg-18-1105-2021.

Berg, B., Ekbohm, G., 1991. Litter mass-loss rates and decomposition patterns in some needle and leaf litter types. Long-term decomposition in a Scots pine forest. VII. Canadian Journal of Botany 69, 1449–1456. https://doi.org/10.1139/b91-187.

Berg, S., Kutra, D., Kroeger, T., Straehle, C.N., Kausler, B.X., Haubold, C., Schiegg, M., Ales, J., Beier, T., Rudy, M., Eren, K., Cervantes, J.I., Xu, B., Beuttenmueller, F., Wolny, A., Zhang, C., Koethe, U., Hamprecht, F.A., Kreshuk, A., 2019. ilastik: interactive machine learning for (bio)image analysis. Nature Methods 16, 1226–1232. https://doi.org/10.1038/s41592-019-0582-9.

Bird, M.I., Wynn, J.G., Saiz, G., Wurster, C.M., McBeath, A., 2015. The pyrogenic carbon cycle. Annual Review of Earth and Planetary Sciences 43, 273–298. https://doi.org/10.1146/annurev-earth-060614-105038.

Bockheim, J.G., 2007. Importance of cryoturbation in redistributing organic carbon in permafrost-affected soils. Soil Science Society of America Journal 71, 1335–1342. https://doi.org/10.2136/sssaj2006.0414N.

Bowring, S.P.K., Jones, M.W., Ciais, P., Guenet, B., Abiven, S., 2022. Pyrogenic carbon decomposition critical to resolving fire's role in the Earth system. Nature Geoscience 15, 135–142. https://doi.org/10.1038/s41561-021-00892-0.

Brodowski, S., John, B., Flessa, H., Amelung, W., 2006. Aggregate-occluded black carbon in soil. European Journal of Soil Science 57, 539–546. https://doi.org/10.1111/j.1365-2389.2006.00807.x.

Chen, Y., Liu, F., Kang, L., Zhang, D., Kou, D., Mao, C., Qin, S., Zhang, Q., Yang, Y., 2021. Large-scale evidence for microbial response and associated carbon release after permafrost thaw. Global Change Biology 1–12. https://doi.org/10.1111/gcb.15487, 00.

Coplen, T.B., 2011. Guidelines and recommended terms for expression of stable-isotope-ratio and gas-ratio measurement results. Rapid Communications in Mass Spectrometry 25, 2538–2560. https://doi.org/10.1002/rcm.5129.

Czimczik, C.I., Masiello, C.A., 2007. Controls on black carbon storage in soils. Global Biogeochemical Cycles 21. https://doi.org/10.1029/2006GB002798.

Ding, Y., Yamashita, Y., Dodds, W.K., Jaffé, R., 2013. Dissolved black carbon in grassland streams: is there an effect of recent fire history? Chemosphere 90, 2557–2562. https://doi.org/10.1016/j.chemosphere.2012.10.098.

Dittmar, T., De Rezende, C.E., Manecki, M., Niggemann, J., Coelho Ovalle, A.R., Stubbins, A., Bernardes, M.C., 2012. Continuous flux of dissolved black carbon from a vanished tropical forest biome. Nature Geoscience 5, 618–622. https://doi.org/10.1038/ngeo1541.

Djukic, I., Kepfer-Rojas, S., Schmidt, I.K., Larsen, K.S., Beier, C., Berg, B., Verheyen, K., Caliman, A., Paquette, A., Gutiérrez-Girón, A., Humber, A., Valdecantos, A., Petraglia, A., Alexander, H., Augustaitis, A., Saillard, A., Fernández, A.C.R., Sousa, A. I., Lillebø, A.I., da Rocha Gripp, A., Francez, A.-J., Fischer, A., Bohner, A., Malyshev, A., Andrić, A., Smith, A., Stanisci, A., Seres, A., Schmidt, A., Avila, A., Probst, A., Ouin, A., Khuroo, A.A., Verstraeten, A., Palabral-Aguilera, A.N., Stefanski, A., Gaxiola, A., Muys, B., Bosman, B., Ahrends, B., Parker, B., Sattler, B., Yang, B., Juráni, B., Erschbamer, B., Ortiz, C.E.R., Christiansen, C.T., Carol Adair, E.,

Meredieu, C., Mony, C., Nock, C.A., Chen, C.-L., Wang, C.-P., Baum, C., Rixen, C., Delire, C., Piscart, C., Andrews, C., Rebmann, C., Branquinho, C., Polyanskaya, D., Delgado, D.F., Wundram, D., Radeideh, D., Ordóñez-Regil, E., Crawford, E., Preda, E., Tropina, E., Groner, E., Lucot, E., Hornung, E., Gacia, E., Lévesque, E., Benedito, E., Davydov, E.A., Ampoorter, E., Bolzan, F.P., Varela, F., Kristöfel, F., Maestre, F.T., Maunoury-Danger, F., Hofhansl, F., Kitz, F., Sutter, F., Cuesta, F., de Almeida Lobo, F., de Souza, F.L., Berninger, F., Zehetner, F., Wohlfahrt, G., Vourlitis, G., Carreño-Rocabado, G., Arena, G., Pinha, G.D., González, G., Canut, G., Lee, H., Verbeeck, H., Auge, H., Pauli, H., Nacro, H.B., Bahamonde, H.A., Feldhaar, H., Jäger, H., Serrano, H.C., Verheyden, H., Bruelheide, H., Meesenburg, H., Jungkunst, H., Jactel, H., Shibata, H., Kurokawa, H., Rosas, H.L., Rojas Villalobos, H.L., Yesilonis, I., Melece, I., Van Halder, I., Quirós, I.G., Makelele, I., Senou, I., Fekete, I., Mihal, I., Ostonen, I., Borovská, J., Roales, J., Shoqeir, J., Lata, J.-C., Theurillat, J.-P., Probst, J.-L., Zimmerman, J., Vijayanathan, J., Tang, J., Thompson, J., Doležal, J., Sanchez-Cabeza, J.-A., Merlet, J., Henschel, J., Neirynck, J., Knops, J., Loehr, J., von Oppen, J., þorláksdóttir, J.S., Löffler, J., Cardoso-Mohedano, J.-G., Benito-Alonso, J.-L., Torezan, J.M., Morina, J.C., Jiménez, J.J., Quinde, J.D., Alatalo, J., Seeber, J., Stadler, J., Kriiska, K., Coulibaly, K., Fukuzawa, K., Szlavecz, K., Gerhátová, K., Lajtha, K., Käppeler, K., Jennings, K.A., Tielbörger, K., Hoshizaki, K., Green, K., Yé, L., Pazianoto, L.H.R., Dienstbach, L., Williams, L., Yahdjian, L., Brigham, L.M., van den Brink, L., Rustad, L., Zhang, L., Morillas, L., Xiankai, L., Carneiro, L.S., Di Martino, L., Villar, L., Bader, M.Y., Morley, M., Lebouvier, M., Tomaselli, M., Sternberg, M., Schaub, M., Santos-Reis, M., Glushkova, M., Torres, M.G.A., Giroux, M.-A., de Graaff, M.-A., Pons, M.-N., Bauters, M., Mazón, M., Frenzel, M., Didion, M., Wagner, M., Hamid, M., Lopes, M.L., Apple, M., Schädler, M., Weih, M., Gualmini, M., Vadeboncoeur, M.A., Bierbaumer, M., Danger, M., Liddell, M., Mirtl, M., Scherer-Lorenzen, M., Růžek, M., Carbognani, M., Di Musciano, M., Matsushita, M., Zhiyanski, M., Puşcaş, M., Barna, M., Ataka, M., Jiangming, M., Alsafran, M., Carnol, M., Barsoum, N., Tokuchi, N., Eisenhauer, N., Lecomte, N., Filippova, N., Hölzel, N., Ferlian, O., Romero, O., Pinto, O.B., Peri, P., Weber, P., Vittoz, P., Turtureanu, P.D., Fleischer, P., Macreadie, P., Haase, P., Reich, P., Petřík, P., Choler, P., Marmonier, P., Muriel, P., Ponette, Q., Guariento, R.D., Canessa, R., Kiese, R., Hewitt, R., Rønn, R., Adrian, R., Kanka, R., Weigel, R., Gatti, R.C., Martins, R.L., Georges, R., Meneses, R.I., Gavilán, R.G., Dasgupta, S., Wittlinger, S., Puijalon, S., Freda, S., Suzuki, S., Charles, S., Gogo, S., Drollinger, S., Mereu, S., Wipf, S., Trevathan-Tackett, S., Löfgren, S., Stoll, S., Trogisch, S., Hoeber, S., Seitz, S., Glatzel, S., Milton, S.J., Dousset, S., Mori, T., Sato, T., Ise, T., Hishi, T., Kenta, T., Nakaji, T., Michelan, T.S., Camboulive, T., Mozdzer, T.J., Scholten, T., Spiegelberger, T., Zechmeister, T., Kleinebecker, T., Hiura, T., Enoki, T., Ursu, T.-M., di Cella, U.M., Hamer, U., Klaus, V.H., Rêgo, V.M., Di Cecco, V., Busch, V., Fontana, V., Piscová, V., Carbonell, V., Ochoa, V., Bretagnolle, V., Maire, V., Farjalla, V., Zhou, W., Luo, W., McDowell, W.H., Hu, Y., Utsumi, Y., Kominami, Y., Zaika, Y., Rozhkov, Y., Kotroczó, Z., Tóth, Z., 2018. Early stage litter decomposition across biomes. Science of the Total Environment 628–629, 1369–1394. https://doi.org/10.1016/j.scitotenv.2018.01.012.

Don, A., Kalbitz, K., 2005. Amounts and degradability of dissolved organic carbon from foliar litter at different decomposition stages. Soil Biology and Biochemistry 37, 2171–2179. https://doi.org/10.1016/j.soilbio.2005.03.019.

Erdozain, M., Freeman, E.C., Ouellet Dallaire, C., Teichert, S., Nelson, H.W., Creed, I.F., 2019. Demand for provisioning ecosystem services as a driver of change in the Canadian boreal zone. Environmental Reviews 27, 166–184. https://doi.org/10.1139/er-2018-0064.

Ernakovich, J.G., Barbato, R.A., Rich, V.I., Schädel, C., Hewitt, R.E., Doherty, S.J., Whalen, E.D., Abbott, B.W., Barta, J., Biasi, C., Chabot, C.L., Hultman, J., Knoblauch, C., Vetter, M.C.Y.L., Leewis, M., Liebner, S., Mackelprang, R., Onstott, T. C., Richter, A., Schütte, U.M.E., Siljanen, H.M.P., Taş, N., Timling, I., Vishnivetskaya, T.A., Waldrop, M.P., Winkel, M., 2022. Microbiome assembly in thawing permafrost and its feedbacks to climate. Global Change Biology gcb, 16231. https://doi.org/10.1111/gcb.16231.

FAO, 2014. World reference base for soil resources 2014. International soil classification system for naming soils and creating legends for soil maps. In: World Soil Resources Reports No. 106. Food and Agriculture Organisation of the United Nations, Rome.

Flannigan, M., Stocks, B., Turetsky, M., Wotton, M., 2009. Impacts of climate change on fire activity and fire management in the circumboreal forest. Global Change Biology 15, 549–560. https://doi.org/10.1111/j.1365-2486.2008.01660.x.

Gentsch, N., Mikutta, R., Alves, R.J.E., Barta, J., Čapek, P., Gittel, A., Hugelius, G., Kuhry, P., Lashchinskiy, N., Palmtag, J., Richter, A., Šantrůčková, H., Schnecker, J., Shibistova, O., Urich, T., Wild, B., Guggenberger, G., 2015a. Storage and transformation of organic matter fractions in cryoturbated permafrost soils across the Siberian Arctic. Biogeosciences 12, 4525–4542. https://doi.org/10.5194/bg-12-4525-2015.

Gentsch, N., Mikutta, R., Shibistova, O., Wild, B., Schnecker, J., Richter, A., Urich, T., Gittel, A., Šantrůčková, H., Bárta, J., Lashchinskiy, N., Mueller, C.W., Fuß, R., Guggenberger, G., 2015b. Properties and bioavailability of particulate and mineral-associated organic matter in Arctic permafrost soils, Lower Kolyma Region, Russia: organic matter stabilization in permafrost soils. European Journal of Soil Science 66, 722–734. https://doi.org/10.1111/ejss.12269.

Gibson, C., Berry, T.D., Wang, R., Spencer, J.A., Johnston, C.T., Jiang, Y., Bird, J.A., Filley, T.R., 2016. Weathering of pyrogenic organic matter induces fungal oxidative enzyme response in single culture inoculation experiments. Organic Geochemistry 92, 32–41. https://doi.org/10.1016/j.orggeochem.2015.12.003.

Gormanns, P., Reckow, S., Poczatek, J.C., Turck, C.W., Lechene, C., 2012. Segmentation of multi-isotope imaging mass spectrometry data for semi-automatic detection of regions of interest. PLoS One 7, e30576. https://doi.org/10.1371/journal.pone.0030576.

Hammes, K., Smernik, R.J., Skjemstad, J.O., Herzog, A., Vogt, U.F., Schmidt, M.W.I., 2006. Synthesis and characterisation of laboratory-charred grass straw (Oryza sativa) and chestnut wood (Castanea sativa) as reference materials for black carbon quantification. Organic Geochemistry 37, 1629–1633. https://doi.org/10.1016/j.orggeochem.2006.07.003.

Hartley, I.P., Garnett, M.H., Sommerkorn, M., Hopkins, D.W., Fletcher, B.J., Sloan, V.L., Phoenix, G.K., Wookey, P.A., 2012. A potential loss of carbon associated with greater plant growth in the European Arctic. Nature Climate Change 2, 875–879. https://doi.org/10.1038/nclimate1575.

Hilscher, A., Knicker, H., 2011a. Carbon and nitrogen degradation on molecular scale of grass-derived pyrogenic organic material during 28 months of incubation in soil. Soil Biology and Biochemistry 43, 261–270. https://doi.org/10.1016/j.soilbio.2010.10.007.

Hilscher, A., Knicker, H., 2011b. Degradation of grass-derived pyrogenic organic material, transport of the residues within a soil column and distribution in soil organic matter fractions during a 28month microcosm experiment. Organic Geochemistry 42, 42–54. https://doi.org/10.1016/j.orggeochem.2010.10.005.

Hobley, E., 2019. Vertical distribution of soil pyrogenic matter: a review. Pedosphere 29, 137–149. https://doi.org/10.1016/S1002-0160(19)60795-2.

Hockaday, W.C., Grannas, A.M., Kim, S., Hatcher, P.G., 2007. The transformation and mobility of charcoal in a fire-impacted watershed. Geochimica et Cosmochimica Acta 71, 3432–3445. https://doi.org/10.1016/j.gca.2007.02.023.

Holden, S.R., Gutierrez, A., Treseder, K.K., 2013. Changes in soil fungal communities, extracellular enzyme activities, and litter decomposition across a fire chronosequence in alaskan boreal forests. Ecosystems 16, 34–46. https://doi.org/10.1007/s10021-012-9594-3.

Hothorn, T., Bretz, F., Westerfall, P., Heoberger, R.M., Schuetzenmeister, A., Scheibe, S., 2021. Multcomp package: simultaneous inference in general parametric models. Version1. 4–17.

Hugelius, G., Tarnocai, C., Broll, G., Canadell, J.G., Kuhry, P., Swanson, D.K., 2013. The Northern Circumpolar Soil Carbon Database: Spatially Distributed Datasets of Soil Coverage and Soil Carbon Storage in the Northern Permafrost Regions 11.

Inagaki, T.M., Possinger, A.R., Grant, K.E., Schweizer, S.A., Mueller, C.W., Derry, L.A., Lehmann, J., Kögel-Knabner, I., 2020. Subsoil organo-mineral associations under contrasting climate conditions. Geochimica et Cosmochimica Acta 270, 244–263. https://doi.org/10.1016/j.gca.2019.11.030.

IPCC, 2021. In: Masson-Delmotte, V., Zhai, P., Pirani, A., Connors, S.L., Péan, C., Berger, S., Caud, N., Chen, L., Goldfarb, L., Gomis, M.I., Huang, M., Leitzell, K., Lonnoy, E., Matthews, J.B.R., Maycock, T.K., Waterfield, T., Yelekçi, O., Yu, R., Zhou, B. (Eds.), Climate Change 2021: The Physical Science Basis. Contribution of Working Group I to the SixthAssessment Report of the Intergovernmental Panel on Climate Change. Cambridge University Press,Cambridge, United Kingdom and New York, NY, USA, p. 2391. https://doi.org/10.1017/9781009157896.

Johnstone, J.F., Hollingsworth, T.N., Chapin III, F.S., 2008. A Key for Predicting Postfire Successional Trajectories in Black Spruce Stands of Interior Alaska. U.S. Department of Agriculture, Forest Service, Pacific Northwest Research Station, Portland, OR.

Jones, M.W., Santín, C., van der Werf, G.R., Doerr, S.H., 2019. Global fire emissions buffered by the production of pyrogenic carbon. Nature Geoscience 12, 742–747. https://doi.org/10.1038/s41561-019-0403-x.

Joseph, S.D., Camps-Arbestain, M., Lin, Y., Munroe, P., Chia, C.H., Hook, J., Van Zwieten, L., Kimber, S., Cowie, A., Singh, B.P., Lehmann, J., Foidl, N., Smernik, R.J., Amonette, J.E., 2010. An investigation into the reactions of biochar in soil. Australian Journal of Soil Research 48, 501–515. https://doi.org/10.1071/SR10009.

Kaiser, C., Meyer, H., Biasi, C., Rusalimova, O., Barsukov, P., Richter, A., 2007. Conservation of soil organic matter through cryoturbation in arctic soils in Siberia. Journal of Geophysical Research 112, G02017. https://doi.org/10.1029/2006JG000258.

Kaiser, K., Guggenberger, G., 2000. The role of DOM sorption to mineral surfaces in the preservation of organic matter in soils. Organic Geochemistry 31, 711–725. https://doi.org/10.1016/S0146-6380(00)00046-2.

Kaiser, K., Kalbitz, K., 2012. Cycling downwards - dissolved organic matter in soils. Soil Biology and Biochemistry 52, 29–32. https://doi.org/10.1016/j.soilbio.2012.04.002.

Kalbitz, K., Solinger, S., Park, J.H., Michalzik, B., Matzner, E., 2000. Controls on the dynamics dissolved organic matter in soils: a review. Soil Science. https://doi.org/10.1097/00010694-200004000-00001.

Kassambara, A., Mundt, F., 2020. Factoextra Package: Extract and Visualize the Results of Multivariate Data Analyses, Version 1.0.7.

Keuskamp, J.A., Dingemans, B.J.J., Lehtinen, T., Sarneel, J.M., Hefting, M.M., 2013. Tea Bag Index: a novel approach to collect uniform decomposition data across ecosystems. Methods in Ecology and Evolution 4, 1070–1075. https://doi.org/10.1111/2041-210X.12097.

Kleber, M., Bourg, I.C., Coward, E.K., Hansel, C.M., Myneni, S.C.B., Nunan, N., 2021. Dynamic interactions at the mineral–organic matter interface. Nature Reviews Earth & Environment. https://doi.org/10.1038/s43017-021-00162-y.

Köchy, M., Hiederer, R., Freibauer, A., 2015. Global distribution of soil organic carbon – Part 1: masses and frequency distributions of SOC stocks for the tropics, permafrost regions, wetlands, and the world. Soils 1, 351–365. https://doi.org/10.5194/soil-1-351-2015.

Kögel-Knabner, I., Guggenberger, G., Kleber, M., Kandeler, E., Kalbitz, K., Scheu, S., Eusterhues, K., Leinweber, P., 2008. Organo-mineral associations in temperate soils: integrating biology, mineralogy, and organic matter chemistry. Journal of Plant Nutrition and Soil Science 171, 61–82. https://doi.org/10.1002/jpln.200700048.

Koranda, M., Kaiser, C., Fuchslueger, L., Kitzler, B., Sessitsch, A., Zechmeister-Boltenstern, S., Richter, A., 2014. Fungal and bacterial utilization of organic

substrates depends on substrate complexity and N availability. FEMS Microbiology Ecology 87, 142–152. https://doi.org/10.1111/1574-6941.12214.
Lehmann, J., Abiven, S., Kleber, M., Pan, G., Singh, B.P., Sohi, S.P., Zimmerman, A.R., 2015. Persistence of biochar in soil. In: Lehmann, J., Joseph, S.D. (Eds.), Biochar for Environmental Management. Routledge, pp. 235–282. https://doi.org/10.4324/9780203762264-17.
Lehmann, J., Rillig, M.C., Thies, J., Masiello, C.A., Hockaday, W.C., Crowley, D., 2011. Biochar effects on soil biota - a review. Soil Biology and Biochemistry 43, 1812–1836. https://doi.org/10.1016/j.soilbio.2011.04.022.
Lützow, M.V., Kögel-Knabner, I., Ekschmitt, K., Matzner, E., Guggenberger, G., Marschner, B., Flessa, H., 2006. Stabilization of organic matter in temperate soils: mechanisms and their relevance under different soil conditions - a review. European Journal of Soil Science 57, 426–445. https://doi.org/10.1111/j.1365-2389.2006.00809.x.
Maestrini, B., Herrmann, A.M., Nannipieri, P., Schmidt, M.W.I., Abiven, S., 2014. Ryegrass-derived pyrogenic organic matter changes organic carbon and nitrogen mineralization in a temperate forest soil. Soil Biology and Biochemistry 69, 291–301. https://doi.org/10.1016/j.soilbio.2013.11.013.
Maestrini, B., Nannipieri, P., Abiven, S., 2015. A meta-analysis on pyrogenic organic matter induced priming effect. GCB Bioenergy 7, 577–590. https://doi.org/10.1111/gcbb.12194.
Major, J., Lehmann, J., Rondon, M., Goodale, C., 2010. Fate of soil-applied black carbon: downward migration, leaching and soil respiration. Global Change Biology 16, 1366–1379. https://doi.org/10.1111/j.1365-2486.2009.02044.x.
Masiello, C.A., Berhe, A.A., 2020. First interactions with the hydrologic cycle determine pyrogenic carbon's fate in the Earth system. Earth Surface Processes and Landforms. https://doi.org/10.1002/esp.4925.
McGuire, A.D., Anderson, L.G., Christensen, T.R., Dallimore, S., Guo, L., Hayes, D.J., Heimann, M., Lorenson, T.D., Macdonald, R.W., Roulet, N., 2009. Sensitivity of the carbon cycle in the Arctic to climate change. Ecological Monographs 79, 523–555. https://doi.org/10.1890/08-2025.1.
Mueller, C.W., Hoeschen, C., Steffens, M., Buddenbaum, H., Hinkel, K., Bockheim, J.G., Kao-Kniffin, J., 2017. Microscale soil structures foster organic matter stabilization in permafrost soils. Geoderma 293, 44–53. https://doi.org/10.1016/j.geoderma.2017.01.028.
Mueller, C.W., Rethemeyer, J., Kao-Kniffin, J., Löppmann, S., Hinkel, K.M., G. Bockheim, J., 2015. Large amounts of labile organic carbon in permafrost soils of northern Alaska. Global Change Biology 21, 2804–2817. https://doi.org/10.1111/gcb.12876.
Peplau, T., Schroeder, J., Gregorich, E., Poeplau, C., 2021. Long-term geothermal warming reduced stocks of carbon but not nitrogen in a subarctic forest soil. Global Change Biology gcb, 15754. https://doi.org/10.1111/gcb.15754.
Pignatello, J.J., Uchimiya, M., Abiven, S., Schmidt, M.W.I., 2015. Evolution of biochar properties in soil. In: Lehmann, Johannes, Joseph, S. (Eds.), Biochar for Environmental Management. Routledge, Abingdon (UK), pp. 195–233. https://doi.org/10.4324/9780203762264-16.
Ping, C.L., Jastrow, J.D., Jorgenson, M.T., Michaelson, G.J., Shur, Y.L., 2015. Permafrost soils and carbon cycling. SOIL 1, 147–171. https://doi.org/10.5194/soil-1-147-2015.
Pingree, M.R.A., DeLuca, T.H., 2017. Function of wildfire-deposited pyrogenic carbon in terrestrial ecosystems. Frontiers in Environmental Science 5, 1–7. https://doi.org/10.3389/fenvs.2017.00053.
Pluchon, N., Vincent, A.G., Gundale, M.J., Nilsson, M.-C., Kardol, P., Wardle, D.A., 2016. The impact of charcoal and soil mixtures on decomposition and soil microbial communities in boreal forest. Applied Soil Ecology 99, 40–50. https://doi.org/10.1016/j.apsoil.2015.11.020.
Ponomarenko, E.V., Anderson, D.W., 2001. Importance of charred organic matter in Black Chernozem soils of Saskatchewan. Canadian Journal of Soil Science 81, 285–297. https://doi.org/10.4141/S00-075.
Preston, C.M., Schmidt, M.W.I., 2006. Black (pyrogenic) carbon : a synthesis of current knowledge and uncertainties with special consideration of boreal regions. Biogeosciences 3, 397–420.
R Core Team, 2021. R Studio.
Reisser, M., Purves, R.S., Schmidt, M.W.I., Abiven, S., 2016. Pyrogenic carbon in soils: a literature-based inventory and a global estimation of its content in soil organic carbon and stocks. Frontiers of Earth Science 4, 1–14. https://doi.org/10.3389/feart.2016.00080.
Rijkers, R., Rousk, J., Aerts, R., Sigurdsson, B.D., Weedon, J.T., 2022. Optimal growth temperature of Arctic soil bacterial communities increases under experimental warming. Global Change Biology gcb, 16342. https://doi.org/10.1111/gcb.16342.
Rumpel, C., Leifeld, J., Santin, C., Doerr, S.H., 2015. Movement of biochar in the environment. In: Lehmann, Johannes, Joseph, S. (Eds.), Biochar for Environmental Management. Routledge, Abingdon (UK), pp. 281–298.
Santín, C., Doerr, S.H., Kane, E.S., Masiello, C.A., Ohlson, M., de la Rosa, J.M., Preston, C. M., Dittmar, T., 2016. Towards a global assessment of pyrogenic carbon from vegetation fires. Global Change Biology 22, 76–91. https://doi.org/10.1111/gcb.12985.
Santos, F., Rice, D.M., Bird, J.A., Berhe, A.A., 2021. Pyrolysis temperature and soil depth interactions determine PyC turnover and induced soil organic carbon priming. Biogeochemistry. https://doi.org/10.1007/s10533-021-00767-x.
Scheel, M., Zervas, A., Jacobsen, C.S., Christensen, T.R., 2022. Microbial community changes in 26,500-year-old thawing permafrost. Frontiers in Microbiology 13, 787146. https://doi.org/10.3389/fmicb.2022.787146.
Schiedung, M., Bellè, S.-L., Malhotra, A., Abiven, S., 2022. Organic carbon stocks, quality and prediction in permafrost-affected forest soils in North Canada. Catena 213, 106194. https://doi.org/10.1016/j.catena.2022.106194.
Schiedung, M., Bellè, S.-L., Sigmund, G., Kalbitz, K., Abiven, S., 2020. Vertical mobility of pyrogenic organic matter in soils: a column experiment. Biogeosciences 17, 6457–6474. https://doi.org/10.5194/bg-17-6457-2020.
Schindelin, J., Rueden, C.T., Hiner, M.C., Eliceiri, K.W., 2015. The ImageJ ecosystem: an open platform for biomedical image analysis: t he I magej E cosystem. Molecular Reproduction and Development 82, 518–529. https://doi.org/10.1002/mrd.22489.
Schuur, E.A.G., McGuire, A.D., Schädel, C., Grosse, G., Harden, J.W., Hayes, D.J., Hugelius, G., Koven, C.D., Kuhry, P., Lawrence, D.M., Natali, S.M., Olefeldt, D., Romanovsky, V.E., Schaefer, K., Turetsky, M.R., Treat, C.C., Vonk, J.E., 2015. Climate change and the permafrost carbon feedback. Nature 520, 171–179. https://doi.org/10.1038/nature14338.
Schweizer, S.A., Hoeschen, C., Schlüter, S., Kögel-Knabner, I., Mueller, C.W., 2018. Rapid soil formation after glacial retreat shaped by spatial patterns of organic matter accrual in microaggregates. Global Change Biology 24, 1637–1650. https://doi.org/10.1111/gcb.14014.
Singh, N., Abiven, S., Maestrini, B., Bird, J.A., Torn, M.S., Schmidt, M.W.I., 2014. Transformation and stabilization of pyrogenic organic matter in a temperate forest field experiment. Global Change Biology 20, 1629–1642. https://doi.org/10.1111/gcb.12459.
Singh, B.P., Cowie, A.L., Smernik, R.J., 2012a. Biochar carbon stability in a clayey soil as a function of feedstock and pyrolysis temperature. Environmental Science and Technology 46, 11770–11778. https://doi.org/10.1021/es302545b.
Singh, N., Abiven, S., Torn, M.S., Schmidt, M.W.I., 2012b. Fire-derived organic carbon in soil turns over on a centennial scale. Biogeosciences 9, 2847–2857. https://doi.org/10.5194/bg-9-2847-2012.
Sistla, S.A., Asao, S., Schimel, J.P., 2012. Detecting microbial N-limitation in tussock tundra soil: implications for Arctic soil organic carbon cycling. Soil Biology and Biochemistry 55, 78–84. https://doi.org/10.1016/j.soilbio.2012.06.010.
Sistla, S.A., Moore, J.C., Simpson, R.T., Gough, L., Shaver, G.R., Schimel, J.P., 2013. Long-term warming restructures Arctic tundra without changing net soil carbon storage. Nature 497, 615–618. https://doi.org/10.1038/nature12129.
Soucémarianadin, L., Reisser, M., Cécillon, L., Barré, P., Nicolas, M., Abiven, S., 2019. Pyrogenic carbon content and dynamics in top and subsoil of French forests. Soil Biology and Biochemistry 133, 12–15. https://doi.org/10.1016/j.soilbio.2019.02.013.
Soucémarianadin, L.N., Quideau, S.A., MacKenzie, M.D., 2014. Pyrogenic carbon stocks and storage mechanisms in podzolic soils of fire-affected Quebec black spruce forests. Geoderma 217–218, 118–128. https://doi.org/10.1016/j.geoderma.2013.11.010.
Soucémarianadin, L.N., Quideau, S.A., MacKenzie, M.D., Munson, A.D., Boiffin, J., Bernard, G.M., Wasylishen, R.E., 2015. Total and pyrogenic carbon stocks in black spruce forest floors from eastern Canada. Organic Geochemistry 82, 1–11. https://doi.org/10.1016/j.orggeochem.2015.02.004.
Spokas, K.A., 2010. Review of the stability of biochar in soils: predictability of O:C molar ratios. Carbon Management 1, 289–303. https://doi.org/10.4155/cmt.10.32.
Spokas, K.A., Novak, J.M., Masiello, C.A., Johnson, M.G., Colosky, E.C., Ippolito, J.A., Trigo, C., 2014. Physical disintegration of biochar: an overlooked process. Environmental Science and Technology Letters 1, 326–332. https://doi.org/10.1021/ez500199t.
Stocks, B.J., Mason, J.A., Todd, J.B., Bosch, E.M., Wotton, B.M., Amiro, B.D., Flannigan, M.D., Hirsch, K.G., Logan, K.A., Martell, D.L., Skinner, W.R., 2002. Large forest fires in Canada, 1959–1997. Journal of Geophysical Research 108. https://doi.org/10.1029/2001jd000484.
Studer, M.S., Künzli, R., Maier, R., Schmidt, M.W.I., Siegwolf, R.T.W., Woodhatch, I., Abiven, S., 2017. The MICE facility–a new tool to study plant–soil C cycling with a holistic approach. Isotopes in Environmental and Health Studies 53, 286–297. https://doi.org/10.1080/10256016.2016.1254209.
Tarnocai, C., Bockheim, J., 2011. Cryosolic soils of Canada: genesis, distribution, and classification. Canadian Journal of Soil Science 91, 749–762. https://doi.org/10.4141/cjss10020.
Tipping, E., Chamberlain, P.M., Fröberg, M., Hanson, P.J., Jardine, P.M., 2012. Simulation of carbon cycling, including dissolved organic carbon transport, in forest soil locally enriched with 14C. Biogeochemistry 108, 91–107. https://doi.org/10.1007/s10533-011-9575-1.
Trofymow, J.A., Moore, T.R., Titus, B., Prescott, C., Morrison, I., Siltanen, M., Smith, S., Fyles, J., Wein, R., Camiré, C., Duschene, L., Kozak, L., Kranabetter, M., Visser, S., 2002. Rates of Litter Decomposition over 6 Years in Canadian Forests: Influence of Litter Quality and Climate, vol. 32, p. 16.
Trumbore, S., 2009. Radiocarbon and soil carbon dynamics. Annual Review of Earth and Planetary Sciences 37, 47–66. https://doi.org/10.1146/annurev.earth.36.031207.124300.
Turetsky, M.R., Abbott, B.W., Jones, M.C., Anthony, K.W., Olefeldt, D., Schuur, E.A.G., Grosse, G., Kuhry, P., Hugelius, G., Koven, C., Lawrence, D.M., Gibson, C., Sannel, A. B.K., McGuire, A.D., 2020. Carbon release through abrupt permafrost thaw. Nature Geoscience 13, 138–143. https://doi.org/10.1038/s41561-019-0526-0.
Wagner, S., Ding, Y., Jaffé, R., 2017. A new perspective on the apparent solubility of dissolved black carbon. Frontiers of Earth Science 5, 1–16. https://doi.org/10.3389/feart.2017.00075.
Wagner, S., Jaffé, R., Stubbins, A., 2018. Dissolved black carbon in aquatic ecosystems. Limnology and Oceanography Letters 168–185. https://doi.org/10.1002/lol2.10076.
Walthert, L., Graf, U., Kammer, A., Luster, J., Pezzotta, D., Zimmermann, S., Hagedorn, F., 2010. Determination of organic and inorganic carbon, δ^{13}C, and nitrogen in soils containing carbonates after acid fumigation with HCl. Journal of Plant Nutrition and Soil Science 173, 207–216. https://doi.org/10.1002/jpln.200900158.

Wild, B., Gentsch, N., Čapek, P., Diáková, K., Alves, R.J.E., Bárta, J., Gittel, A., Hugelius, G., Knoltsch, A., Kuhry, P., Lashchinskiy, N., Mikutta, R., Palmtag, J., Schleper, C., Schnecker, J., Shibistova, O., Takriti, M., Torsvik, V.L., Urich, T., Watzka, M., Šantrůčková, H., Guggenberger, G., Richter, A., 2016. Plant-derived compounds stimulate the decomposition of organic matter in arctic permafrost soils. Scientific Reports 6, 25607. https://doi.org/10.1038/srep25607.

Wild, B., Schnecker, J., Alves, R.J.E., Barsukov, P., Bárta, J., Čapek, P., Gentsch, N., Gittel, A., Guggenberger, G., Lashchinskiy, N., Mikutta, R., Rusalimova, O., Šantrůčková, H., Shibistova, O., Urich, T., Watzka, M., Zrazhevskaya, G., Richter, A., 2014. Input of easily available organic C and N stimulates microbial decomposition of soil organic matter in arctic permafrost soil. Soil Biology and Biochemistry 75, 143–151. https://doi.org/10.1016/j.soilbio.2014.04.014.

Wild, B., Schnecker, J., Bárta, J., Čapek, P., Guggenberger, G., Hofhansl, F., Kaiser, C., Lashchinsky, N., Mikutta, R., Mooshammer, M., Šantrůčková, H., Shibistova, O., Urich, T., Zimov, S.A., Richter, A., 2013. Nitrogen dynamics in turbic Cryosols from siberia and Greenland. Soil Biology and Biochemistry 67, 85–93. https://doi.org/10.1016/j.soilbio.2013.08.004.

Wilhelm, R.C., Lynch, L., Webster, T.M., Schweizer, S., Inagaki, T.M., Tfaily, M.M., Kukkadapu, R., Hoeschen, C., Buckley, D.H., Lehmann, J., 2022. Susceptibility of new soil organic carbon to mineralization during dry-wet cycling in soils from contrasting ends of a precipitation gradient. Soil Biology and Biochemistry 169, 108681. https://doi.org/10.1016/j.soilbio.2022.108681.

Xu, L., Myneni, R.B., Chapin III, F.S., Callaghan, T.V., Pinzon, J.E., Tucker, C.J., Zhu, Z., Bi, J., Ciais, P., Tømmervik, H., Euskirchen, E.S., Forbes, B.C., Piao, S.L., Anderson, B.T., Ganguly, S., Nemani, R.R., Goetz, S.J., Beck, P.S.A., Bunn, A.G., Cao, C., Stroeve, J.C., 2013. Temperature and vegetation seasonality diminishment over northern lands. Nature Climate Change 3, 581–586. https://doi.org/10.1038/nclimate1836.

Xu, W., Elberling, B., Ambus, P.L., 2022. Pyrogenic organic matter as a nitrogen source to microbes and plants following fire in an Arctic heath tundra. Soil Biology and Biochemistry 170, 108699. https://doi.org/10.1016/j.soilbio.2022.108699.

Zhang, X., Flato, G., Kirchmeier-Young, M., Vincent, L., Wan, H., Wang, X., Rong, R., Fyfe, J., Kharin, V.V., 2019. Changes in temperature and precipitation across Canada; chapter 4. In: Bush, E., Lemmen, D.S. (Eds.), Canada's Changing Climate Report. Government of Canada, Ottawa, Ontario, pp. 112–193. https://doi.org/10.4095/314614.

Zimmerman, A.R., 2010. Abiotic and microbial oxidation of laboratory-produced black carbon (biochar). Environmental Science & Technology 44, 1295–1301. https://doi.org/10.1021/es903140c.